Provided for non-commercial research and educational use only.
Not for reproduction, distribution or commercial use.

This chapter was originally published in the book *Progress in Optics*. The copy attached is provided by Elsevier for the author's benefit and for the benefit of the author's institution, for non-commercial research, and educational use. This includes without limitation use in instruction at your institution, distribution to specific colleagues, and providing a copy to your institution's administrator.

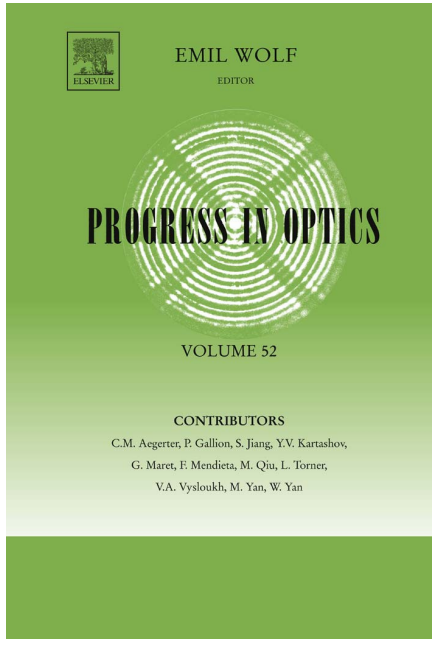

All other uses, reproduction and distribution, including without limitation commercial reprints, selling or licensing copies or access, or posting on open internet sites, your personal or institution's website or repository, are prohibited. For exceptions, permission may be sought for such use through Elsevier's permissions site at:
http://www.elsevier.com/locate/permissionusematerial

From Min Yan, Wei Yan, Min Qiu. Invisibility Cloaking by Coordinate Transformation. In: Emil Wolf, editor: Progress in Optics, Vol 52, Hungary: Elsevier; 2009, p. 261–304.
ISBN: 978-0-444-53350-0
© Copyright 2009 Elsevier B.V.
Elsevier

Author's personal copy

CHAPTER 4

Invisibility Cloaking by Coordinate Transformation

Min Yan, Wei Yan and **Min Qiu**[1]

Department of Microelectronics and Applied Physics, Royal Institute of Technology (KTH), Electrum 229, 164 40 Kista, Sweden

Contents

1. INTRODUCTION

Recently the advent of artificial electromagnetic (EM) materials, referred to as *metamaterials* (Smith, Pendry and Wiltshire, 2004; Shalaev, 2006), has opened up many new ways for us to interact with or control EM waves. EM phenomena that do not exist in nature have been demonstrated experimentally. Negative refraction (Shelby, Smith and Schultz, 2001)

[1] Tel.: +46 8 7904068; fax: +46 8 7904090.
E-mail address: min@kth.se (M. Qiu).

Progress in Optics, Volume 52 © 2009 Elsevier B.V.
ISSN 0079-6638, DOI 10.1016/S0079-6638(08)00006-1 All rights reserved.

Author's personal copy

and negative-index slab superlenses (Pendry, 2000) are representative applications of this class of engineered materials. With metamaterials, not only are we able to tailor their permittivity and permeability values at will, but we also have precise control over the anisotropy of the material and how all parameters vary with spatial location. While it is not a problem to engineer each individual metamaterial unit, placing the units in the appropriate order to achieve a desired macroscopic optical phenomenon remains a challenge. In simple language, with trees of various sizes and color at our disposal, how does one create an enchanting forest? The recently proposed coordinate transformation method provides an ideal recipe for solving such a design problem.

This paper focuses on the design of a special type of EM device, the invisibility cloak, deduced from the coordinate transformation technique. The structure of our presentation is as follows. First, the theory of coordinate transformation for Maxwell's equations will be summarized in Section 2. The principle and formation of invisibility cloaks based the technique of coordinate transformation will be described in Section 3. In Section 4, the perfect invisibility performance of arbitrarily shaped cloaks will then be confirmed by using full-wave analytical analysis. The material parameters of arbitrarily shaped cloaks will be examined closely. After covering the general arbitrarily shaped cloaks, we will study cylindrical and spherical cloaks (Sections 5 and 6) in detail. Special attention will be paid to the cylindrical invisibility cloak since it is arguably the simplest structure in terms of realization. Some practical issues concerning invisibility cloaks, as well as other related studies, will be discussed in Section 7. Finally, a summary will be given in Section 8.

2. COORDINATE TRANSFORMATION IN ELECTROMAGNETISM

The theory of transformation optics has its roots in the covariance property of the Maxwell equations. The best mathematical description of such a covariance property is by using differential geometry (Post, 1962), a machinery that is commonly adopted for formulating the theory of general relativity (Leonhardt and Philbin, 2006). Strict derivation of the theory of transformation optics in 4D Minkowski space can be found in Leonhardt and Philbin (2008). In this paper we directly lay out the most important conclusions in a mathematically more accessible form. Since most practical applications of transformation optics are static or moving slowly compared to the speed of light, we can always choose our working frame properly, and therefore can consider only spatial coordinate transformation. Time will not be involved in coordinate transformations discussed in this paper.

Author's personal copy

In a flat 3D Euclidean space, the macroscopic Maxwell's equation can be written as

$$\nabla \times \mathbf{E} = -\frac{\partial \mathbf{B}}{\partial t}, \quad \nabla \times \mathbf{H} = \frac{\partial \mathbf{D}}{\partial t} + \mathbf{j}, \quad \nabla \cdot \mathbf{D} = \rho, \quad \nabla \cdot \mathbf{B} = 0. \tag{1}$$

E and **H** are the electric and magnetic fields, respectively; **D** and **B** are the electric and magnetic flux densities, respectively; **j** is the electric current density; and ρ is the charge density. The Maxwell equations are completed by two constitutive relations

$$\mathbf{D} = \epsilon_0 \overline{\overline{\varepsilon}} \cdot \mathbf{E}, \quad \mathbf{B} = \mu_0 \overline{\overline{\mu}} \cdot \mathbf{H}, \tag{2}$$

where $\overline{\overline{\varepsilon}}$ and $\overline{\overline{\mu}}$ are 3×3 permittivity and permeability tensors, respectively. Consider a coordinate transformation from the Cartesian space (x, y, z) to an arbitrary curved space described by coordinates (q_1, q_2, q_3) with

$$x = f_1(q_1, q_2, q_3), \quad y = f_2(q_1, q_2, q_3), \quad z = f_3(q_1, q_2, q_3). \tag{3}$$

The Jacobian transformation matrix Λ is written as

$$\Lambda = \begin{bmatrix} \dfrac{\partial x}{\partial q_1} & \dfrac{\partial x}{\partial q_2} & \dfrac{\partial x}{\partial q_3} \\ \dfrac{\partial y}{\partial q_1} & \dfrac{\partial y}{\partial q_2} & \dfrac{\partial y}{\partial q_3} \\ \dfrac{\partial z}{\partial q_1} & \dfrac{\partial z}{\partial q_2} & \dfrac{\partial z}{\partial q_3} \end{bmatrix}. \tag{4}$$

The length of a line element in the transformed space is given by $\mathrm{d}l^2 = [\mathrm{d}q_1, \mathrm{d}q_2, \mathrm{d}q_3]\mathbf{g}[\mathrm{d}q_1, \mathrm{d}q_2, \mathrm{d}q_3]^T$, where $\mathbf{g} = \Lambda^T \Lambda$ is the space metric tensor, and the superscript "T" denotes matrix transposition. The volume of a space element is expressed as $\mathrm{d}v = \det(\Lambda)\mathrm{d}q_1\mathrm{d}q_2\mathrm{d}q_3$, where $\det(\Lambda)$ represents the determinant of Λ.

Then Maxwell's equations in the curved space can take their invariant form as (Ward and Pendry, 1996)

$$\nabla_q \times \widehat{\mathbf{E}} = -\frac{\partial \widehat{\mathbf{B}}}{\partial t}, \quad \nabla_q \times \widehat{\mathbf{H}} = \frac{\partial \widehat{\mathbf{D}}}{\partial t} + \widehat{\mathbf{j}}, \quad \nabla_q \cdot \widehat{\mathbf{D}} = \widehat{\rho}, \quad \nabla_q \cdot \widehat{\mathbf{B}} = 0 \tag{5}$$

with new constitutive equations as

$$\widehat{\mathbf{D}} = \epsilon_0 \widehat{\overline{\overline{\varepsilon}}} \cdot \widehat{\mathbf{E}}, \quad \widehat{\mathbf{B}} = \mu_0 \widehat{\overline{\overline{\mu}}} \cdot \widehat{\mathbf{H}}, \tag{6}$$

Author's personal copy

where all variables in the new coordinate system have been denoted by a hat. In order to keep such invariant forms of Maxwell's equations, the new permittivity and permeability tensors have to fulfill

$$\widehat{\overline{\overline{\varepsilon}}} = \det(\Lambda)(\Lambda)^{-1}\overline{\overline{\varepsilon}}\Lambda^{-T}, \quad \widehat{\overline{\overline{\mu}}} = \det(\Lambda)(\Lambda)^{-1}\overline{\overline{\mu}}\Lambda^{-T}, \tag{7}$$

where the superscript "-1" denotes matrix inversion, and "$-T$" denotes matrix transposition *and* inversion. The fields and the sources in the new coordinate system can be directly obtained from their respective distributions in the original coordinate system as

$$\widehat{\mathbf{E}} = \Lambda^T\mathbf{E}, \quad \widehat{\mathbf{H}} = \Lambda^T\mathbf{H}, \tag{8}$$

$$\widehat{\mathbf{j}} = \det(\Lambda)(\Lambda)^{-1}\mathbf{j}, \quad \widehat{\rho} = \det(\Lambda)\rho. \tag{9}$$

It is seen from the above equations that a change of coordinate system does not prevent us from solving exactly the same set of equations, provided that the permittivity and permeability tensors have been defined differently.

When the permittivity and permeability in the original Cartesian coordinate system are isotropic, the newly obtained permittivity and permeability in Equation (7) can be further written as

$$\widehat{\overline{\overline{\varepsilon}}} = \det(\Lambda)g^{-1}\varepsilon, \quad \widehat{\overline{\overline{\mu}}} = \det(\Lambda)g^{-1}\mu. \tag{10}$$

It should be mentioned that more than one coordinate transformation can take place successively. The relationship between the EM system in the initial coordinates and that in the final coordinates can be characterized by the global Jacobian coordinate transformation matrix, which is computed by multiplying Jacobian matrices for individual coordinate transformations (Zolla, Guenneau, Nicolet and Pendry, 2007). The global Jacobian matrix can then be applied for obtaining material and field distributions in the final coordinate system. One useful application of this strategy occurs when the coordinate transformation can be described much more easily in some coordinate system other than the Cartesian system. As an example, under a cylindrical coordinate system, a coordinate transformation may involve only a mapping of the radial coordinate component, i.e. from (r, θ, z) to (r', θ', z') with $\theta = \theta'$ and $z = z'$. To interpret the transformation in a Cartesian coordinate system, the global Jacobian transformation matrix is

$$\Lambda = \Lambda_{xr}\Lambda_{rr'}\Lambda_{r'x'}, \tag{11}$$

Author's personal copy

where Λ_{xr} characterizes the change from Cartesian coordinates to cylindrical coordinates, $\Lambda_{rr'}$ characterizes the transformation from the original cylindrical coordinates to new cylindrical coordinates, and $\Lambda_{r'x'}$ denotes change of the new cylindrical coordinates back to Cartesian coordinates.

There are notably two important applications of the covariance property of electrodynamics described above. First, the geometries of some complex structures can be simplified greatly if they are described in their "natural" coordinates. Such an alternative geometrical description of complex structures can facilitate more efficient theoretical treatment of the EM problem, usually at the expense of more complex material parameter distributions. One example is to numerically deal with a helically twisted optical waveguide (Nicolet, Zolla and Guenneau, 2004; Shyroki, 2008), where a 3D problem can be simplified into a 2D one. The second application of the covariance property is for designing optical devices that can achieve novel phenomena. From the equations presented above, the new EM field, if interpreted from the original Cartesian coordinate system, will appear distorted. The field distortion is characterized by the Jacobian transformation matrix, and that in turn is characterized by how we choose the curved coordinate system. It should be noticed that the structure, including its material parameters obtained through coordinate transformation in the curved coordinate system, has been interpreted back on to the original Cartesian system. This is the so-called "material interpretation" of the covariance property of Maxwell's equations (Schurig, Pendry and Smith, 2006b). When the newly obtained material parameters are interpreted in the original Cartesian coordinate system, one obtains an effective medium, which is referred to as the *transformation medium*. The transformation medium mimics the effect of curved spatial coordinates, and facilitate bending of light. In many cases, distortion of the EM field is what most optical devices are trying to achieve. Typical examples include waveguide bends, where change of beam direction is desired to facilitate dense optical integration, and lenses, where a spatially divergent field from a point source is refocused to a spot, etc. The fact that we are able to set out from certain desired EM wave behaviour and obtain some specific complex medium using the method of coordinate transformation suggests that designs of many novel devices can be within our reach. The metamaterial technology would complete the final fabrication step according to derived material parameter distributions.

In the published literature, there are several proposed devices based on the theory of coordinate transformation, namely the invisibility cloak (Leonhardt, 2006; Pendry, Schurig and Smith, 2006), perfect lenses (Leonhardt and Philbin, 2006; Schurig, Pendry and Smith, 2007; Tsang

Author's personal copy

and Psaltis, 2008; Kildishev and Shalaev, 2008; Kildishev and Narimanov, 2007; Yan, Yan and Qiu, 2008a), EM field rotator (Chen and Chan, 2007), EM concentrators (Rahm, Schurig, Roberts, Cummer, Smith and Pendry, 2008b), EM beam splitter (Rahm, Cummer, Schurig, Pendry and Smith, 2008a), antenna (Kong, Wu, Kong, Huangfu, Xi and Chen, 2007), and EM wormholes (Greenleaf, Kurylev, Lassas and Uhlmann, 2007a) etc. When time is also involved in the transformation, as in Minkowski space, the theory of coordinate transformation also helps to explain the EM analogues of the event horizon as well as the so-called optical Aharonov-Bohm effect (Leonhardt and Philbin, 2006). In this paper, we will focus particularly on the EM cloaking devices. Not only because the fact that the proposal of the EM cloaking phenomenon has revived the covariance principle of electrodynamics in the design of novel devices, but also because the invisibility cloaking technology itself is of great interest to many for military and civilian applications. Invisibility cloaking has remained as a very popular concept in the world of science fiction or fantasy novels. The possibility of an EM invisibility device has recently inspired theoretical investigations on cloaking of sound (Milton, Briane and Willis, 2006; Cummer and Schurig, 2007; Cummer, Popa, Schurig, Smith, Pendry, Rahm and Starr, 2008; Norris, 2008; Chen, Yang, Luo and Ma, 2008), matter waves (Zhang, Genov, Sun and Zhang, 2008d; Greenleaf, Kurylev, Lassas and Uhlmann, 2008), and even surface wave in a liquid (Farhat, Enoch, Guenneau and Movchan, 2008).

It should be mentioned that some studies on invisibility cloaking existed before the paper by Pendry and his co-workers (Pendry, Schurig and Smith, 2006). Notably, a technique similar to the coordinate transformation was deployed for achieving invisibility in the static limit (Greenleaf, Lassas and Uhlmann, 2003). Furthermore, there have been proposals on invisibility cloaking devices based on techniques other than the coordinate transformation approach. Among such works, surface plasmon resonance has been utilized to hide small particles (see e.g. Alù and Engheta (2005); Milton and Nicorovici (2006); Alù and Engheta (2008)), and also in Miller (2006) a network of sensors and active sources are used to achieve invisibility.

3. PRINCIPLE AND CONSTRUCTION OF INVISIBILITY CLOAKS

The possibility of invisibility cloaking arises when a newly chosen curved coordinate system contains a void region. A simple way to visualize this is to lay out the curved coordinate lines in the original Cartesian coordinate system according to the relation as defined by Equation (3) (in fact, it will be much clearer to see from the inverse of the functions, i.e. $q_1 = q_1(x, y, z)$ etc). A spatial region in the Cartesian space that

Author's personal copy

is not passed through by any curved coordinate lines is a void region. This situation is illustrated in Figure 1, where Figure 1(a) and (b) depict coordinates before and after transformation, respectively. Notice that the coordinates change only for a finite spatial region bounded by S_1 in both panels. As a consequence, the material outside S_1 remains the same in Figure 1(a) and (b) due to the identity transformation in that region of space. In Figure 1(b), a void region has appeared, which is bounded by the boundary S_2. The void region corresponds to a point of zero size (or a line, if the structure is invariant in the direction normal to the page) in the original coordinate system shown in Figure 1(a). The annular shape, as bounded by S_1 and S_2 in Figure 1(b), is electromagnetically equivalent to the region bounded by S_1 in Figure 1(a). However their material parameters are different owing to the change of coordinates. A medium obtained through coordinate transformation, such as the annular shape in Figure 1(b), is referred to as a transformation medium. Due to the presence of a void region in Figure 1(b), hiding of objects is possible since light will be unable to penetrate the void region. In the case where the original space in Figure 1(a) is empty, the resulting transformation medium is an object with anisotropic material properties, which is invisible and at the same time provides shielding to other objects enclosed in S_2.

As a side note, at exactly the S_1 boundary in Figure 1, the transformed coordinate components are kept the same as the original Cartesian coordinate components, i.e. $x|_{S_1} = q_1|_{S_1}$ etc. In Yan, Yan and Qiu (2008b), such coordinate continuation at a finite transformation medium's boundary is found to be a necessary and sufficient condition in order to achieve an impedance matching condition for an arbitrarily shaped structure.

The method of coordinate transformation can not only design complex transformation media, it also directly defines the field profile in the transformation media through Equation (8). Here, for ease of illustration, we consider the systems shown in Figure 1 which are two-dimensional, i.e. they are invariant in the direction normal to the page (say z). Under this condition, E_z, the electric field in original space and $E'_{z'}$, the electric field in transformed space should be equal in amplitude, except that the distribution of $E'_{z'}$ should be distorted compared with E_z according to the particular coordinate transformation deployed. Assume also that the original space is free space. In the case of a right-propagating plane wave with E_z polarization, the electric field distributions before and after transformation are shown in Figure 2(a) and (b), respectively.

In short, to construct a cloak, one usually starts by compressing a finite space whilst keeping the outer boundary S_1 unchanged, and the inner boundary S_2 is obtained by blowing up a line (straight or curved) or a point. Thus the cloaks are divided into two classes: *line-transformed cloaks*

Author's personal copy

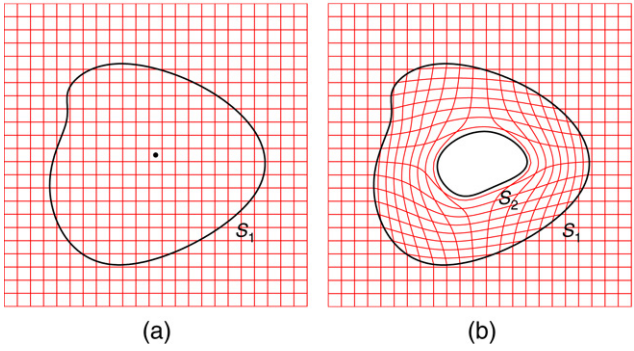

FIGURE 1 Illustration of coordinate transformation for obtaining a cloak of virtually arbitrary shape in 2D. (a) Original Cartesian coordinates; (b) Transformed curved coordinates. Coordinate lines before and after transformation are in red. The region bounded by S_1 and S_2 is the transformation medium that constitutes a cloak

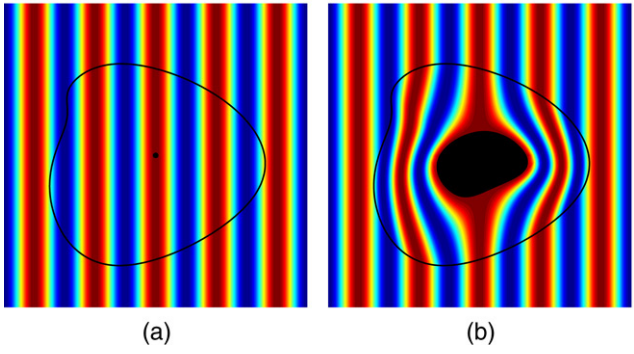

FIGURE 2 E_z field before transformation. (b) E_z field after transformation

and *point-transformed* cloaks. The permittivity and permeability tensors of the cloak in a Cartesian coordinate system are given in Equation (7).

4. ARBITRARILY-SHAPED INVISIBILITY CLOAKS

The material parameters of an arbitrarily-shaped cloak are very complex. The medium is not only anisotropic, but also spatially gradient. In this section, we will examine the performance and properties of such invisibility cloaks using an analytical technique. Both the line-transformed cloak and the point-transformed cloak are studied. Analytical study of such arbitrarily-shaped cloaks is possible since the eigenfunctions of the

Author's personal copy

wave equations in the cloak medium are in fact quite simple, and related to the eigenfunctions in the original space through Equation (8).

In order to achieve *perfect invisibility*, the cloak should be able to exclude light from a protected object without perturbing the outer field. Thus for a perfect invisibility cloak, two conditions must be fulfilled: (1) at the outer boundary S_1, external incident light should excite no reflection; (2) at the inner boundary S_2, no reflection is excited, and no light can penetrate the cloaked region. In the following subsections, we will prove the invisibility of the cloak by investigating the behaviour of waves at the cloak's outer and inner boundaries. For simplicity, the invisibility cloak is considered to be placed in free space. That is, the relative permittivity and permeability of the cloak in Equation (10) will be simplified to

$$\widehat{\overline{\overline{\varepsilon}}} = \widehat{\overline{\overline{\mu}}} = \det(\Lambda)\mathbf{g}^{-1}. \tag{12}$$

4.1 Outer Boundary of Cloak

In this subsection, it will be proved that no reflection is excited at the outer boundary for either line-transformed cloaks or point-transformed cloaks. The transmitted electric field $\widehat{\mathbf{E}}^i$ and magnetic field $\widehat{\mathbf{H}}^i$ (before interacting with the inner boundary S_2) are expressed as

$$\widehat{\mathbf{E}}^i = \Lambda^T \mathbf{E}^i, \quad \widehat{\mathbf{H}}^i = \Lambda^T \mathbf{H}^i, \tag{13}$$

where $\mathbf{E}^i$ and $\mathbf{H}^i$ represent the electric and magnetic fields of the external incident waves. According to Equation (8), it is easily seen that the fields expressed in Equation (13) satisfy Maxwell's equations in the cloak medium. Thus in order to prove that no reflection is excited at S_1, one only needs to confirm that the tangential components of $\mathbf{E}^i$ ($\mathbf{H}^i$) and $\widehat{\mathbf{E}}^i$ ($\widehat{\mathbf{H}}^i$) remain continuous across S_1.

Decomposing $\widehat{\mathbf{E}}^i$ and $\widehat{\mathbf{H}}^i$ into $\widehat{\mathbf{E}}^i = [\widehat{E}^i_n, \widehat{E}^i_{t_1}, \widehat{E}^i_{t_2}]$ and $\widehat{\mathbf{H}}^i = [\widehat{H}^i_n, \widehat{H}^i_{t_1}, \widehat{H}^i_{t_2}]$, where the subscript n represents the surface normal in the direction pointing outward from S_1; t_1 and t_2 represent two surface tangent directions, which are perpendicular to each other, Equation (13) can be equivalently expressed as

$$\begin{bmatrix} \widehat{E}^i_n \\ \widehat{E}^i_{t_1} \\ \widehat{E}^i_{t_2} \end{bmatrix} = [\widehat{n}, \widehat{t}_1, \widehat{t}_2]^{-1} \Lambda^T \mathbf{E}^i, \quad \begin{bmatrix} \widehat{H}^i_n \\ \widehat{H}^i_{t_1} \\ \widehat{H}^i_{t_2} \end{bmatrix} = [\widehat{n}, \widehat{t}_1, \widehat{t}_2]^{-1} \Lambda^T \mathbf{H}^i, \tag{14}$$

Author's personal copy

where $\widehat{n}$, $\widehat{t_1}$, $\widehat{t_2}$ represent the unit vectors in n, t_1, and t_2 directions, respectively.

At the outer boundary S_1, $q_1 = x$, $q_2 = y$, and $q_3 = z$. So $f_i(q_1, q_2, q_3) - q_i = 0$ $(i = 1, 2, 3)$ characterize the outer boundary S_1. Therefore, it is obvious that the vectors $\nabla_q f_i - \widehat{C}_i$ $(i = 1, 2, 3)$ lie in the same line as the normal direction n of S_1, where $\widehat{C}_1 = \widehat{x}$, $\widehat{C}_2 = \widehat{y}$, and $\widehat{C}_3 = \widehat{z}$. For the special case when $\nabla_q f_i - \widehat{C}_i = 0$, $\nabla_q f_i - \widehat{C}_i$ can be expressed as $0\widehat{n}$, i.e., the vector with zero magnitude in the n direction. Therefore, Λ^T on S_1 can be expressed as

$$\Lambda^T = [F_1\widehat{n} + \widehat{x}, F_2\widehat{n} + \widehat{y}, \widehat{F_3}\widehat{n} + \widehat{z}], \tag{15}$$

with

$$|F_i| = \sqrt{\left(\frac{\partial f_i}{\partial q_i} - 1\right)^2 + \left(\frac{\partial f_i}{\partial q_j}\right)^2 + \left(\frac{\partial f_i}{\partial q_k}\right)^2}, \tag{16}$$

where $i, j, k = 1, 2, 3$ and $i \neq j \neq k$; $F_i = |F_i|$ when the direction of $\nabla_q f_i - \widehat{C}_i$ is the same as the n direction, and $F_i = -|F_i|$ if the direction of $\nabla_q f_i - \widehat{C}_i$ is opposite to the n direction. Substituting Equation (15) into Equation (14) and noticing that $\widehat{n}$, $\widehat{t_1}$, and $\widehat{t_2}$ are orthogonal to each other, it is easily shown that at S_1

$$\widehat{E}^i_{t_1} = \mathbf{E}^i \cdot \widehat{t_1}, \quad \widehat{H}^i_{t_1} = \mathbf{H}^i \cdot \widehat{t_1}, \tag{17}$$

$$\widehat{E}^i_{t_2} = \mathbf{E}^i \cdot \widehat{t_2}, \quad \widehat{H}^i_{t_2} = \mathbf{H}^i \cdot \widehat{t_2}, \tag{18}$$

which indicates that the tangential components of $\mathbf{E}^i$ $(\mathbf{H}^i)$ and $\widehat{\mathbf{E}}^i$ $(\widehat{\mathbf{H}}^i)$ are continuous across S_1. Thus, it is proved that no reflection is excited at the outer boundary for both line-transformed cloaks and point-transformed cloaks.

4.2 Inner Boundary of Cloak

In this subsection, it will be proved that at the inner boundary S_2, no reflection is excited and no field can penetrate into the cloaked region. As discussed in the above subsection, the inner boundary is constructed by blowing up a line or a point, as seen in Figure 3(a) and (b). So in the following, two cases: (1) line-transformed cloaks, (2) point-transformed cloaks, will be discussed separately.

4.2.1 Line-transformed Cloaks

Assume that $x = b_1(s)$, $y = b_2(s)$ and $z = b_3(s)$ characterize the line, which is mapped to the inner boundary S_2. Thus, we have $f_1(q_1, q_2, q_3) = b_1(s)$

Author's personal copy

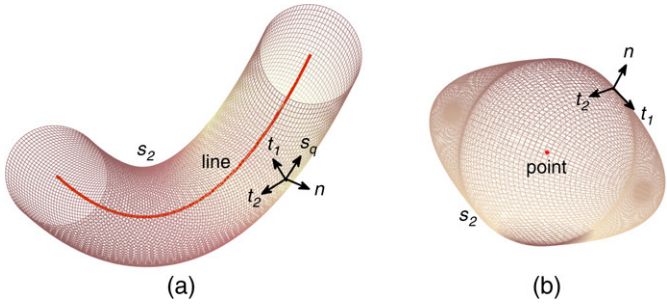

FIGURE 3 Illustration of inner boundary of cloak for (a) a line-transformed cloak; (b) a point-transformed cloak

and $f_2(q_1, q_2, q_3) = b_2(s)$, and $f_3(q_1, q_2, q_3) = b_3(s)$ at S_2. Each point (b_1, b_2, b_3) on the line maps to a closed curve on S_2. The parameter s can be expressed as a function of q_1, q_2, q_3 with $s = u(q_1, q_2, q_3)$. $\nabla_q s = \partial u/\partial q_1 \widehat{x} + \partial u/\partial q_2 \widehat{y} + \partial u/\partial q_3 \widehat{z}$ is the gradient of s, which points in the direction of the greatest rate of increase of s. For $\nabla_q b_i$, we have $\nabla_q b_i = \partial b_i/\partial s \nabla_q s$, where $i = 1, 2, 3$. Thus, the vectors $\nabla_q b_i$ and $\nabla_q s$ have the same (or antiparallel) direction.

For ease of discussion, we again decompose the transmitted fields expressed in Equation (13) at the inner boundary as $\widehat{\mathbf{E}}^i = [\widehat{E}^i_n, \widehat{E}^i_{t_1}, \widehat{E}^i_{t_2}]$, $\widehat{\mathbf{H}}^i = [\widehat{H}^i_n, \widehat{H}^i_{t_1}, \widehat{H}^i_{t_2}]$, where the subscript n denotes the surface normal direction pointing outward from S_2; t_1 and t_2 denote two surface tangent directions of S_2, with t_1 perpendicular to the plane determined by two vectors in n and $\nabla_q s$ directions, and t_2 perpendicular to t_1. Since s varies on the surface S_2, the direction of $\nabla_q s$ (denoted by s_q in Figure 3(b)) should not be parallel to the normal direction of S_2. Thus, the plane determined by the vectors in n and $\nabla_q s$ directions always exists. The n, t_1, and t_2 directions are unique, as illustrated in Fig. 3(a). $\widehat{\mathbf{E}}^i$ and $\widehat{\mathbf{H}}^i$ at S_2 can also be expressed in Equation (14), however, with different definitions of n, t_1 and t_2. Since $f_i(q_1, q_2, z) - b_i(s) = 0$ characterizes the inner boundary S_2, $\nabla_q f_i - \nabla_q b_i$ characterizes the normal direction of S_2. Then Λ^T at S_2 can be written as

$$\Lambda^T = [F_1 \widehat{n} + \nabla_q b_1, F_2 \widehat{n} + \nabla_q b_2, F_3 \widehat{n} + \nabla_q b_3], \tag{19}$$

with

$$|F_i| = \sqrt{\sum_{j=1}^{3} (\partial f_i/\partial q_j - \partial b_i/\partial q_j)^2}, \tag{20}$$

Author's personal copy

where $F_i = |F_i|$ when the direction of $\nabla_q f_i - \nabla_q b_i$ is the same as the direction of n, and $F_i = -|F_i|$ when the direction of $\nabla_q f_i - \nabla_q b_i$ is opposite to the direction of n.

Notice that t_1 is orthogonal to both n and s_q, when $\widehat{s}$ denotes the unit vector in the direction of $\nabla_q s$. Substituting Equation (19) into Equation (14), it is easily derived that at the inner boundary

$$\widehat{E}^i_{t1} = \widehat{H}^i_{t1} = 0. \tag{21}$$

However, the other components of the fields are not zero. In particular,

$$\widehat{E}^i_{t2} = (\widehat{s} \cdot \widehat{t_2})[B_1, B_2, B_3]\mathbf{E}^i, \tag{22}$$
$$\widehat{H}^i_{t2} = (\widehat{s} \cdot \widehat{t_2})[B_1, B_2, B_3]\mathbf{H}^i, \tag{23}$$
$$\widehat{E}^i_{n} = [F_1 + B_1(\widehat{s} \cdot \widehat{n}), F_2 + B_2(\widehat{s} \cdot \widehat{n}), F_3 + B_3(\widehat{s} \cdot \widehat{n})]\mathbf{E}^i, \tag{24}$$
$$\widehat{H}^i_{n} = [F_1 + B_1(\widehat{s} \cdot \widehat{n}), F_2 + B_2(\widehat{s} \cdot \widehat{n}), F_3 + B_3(\widehat{s} \cdot \widehat{n})]\mathbf{H}^i, \tag{25}$$

with

$$B_i = \sqrt{\sum_{j=1}^{3} (\partial b_i / \partial q_j)^2}. \tag{26}$$

To further investigate how the waves interact with the inner boundary, the values of the permittivity and permeability at S_2 are needed. Considering Λ as expressed in Equation (19), it is easily seen that $\Lambda\widehat{t_1} = 0$, indicating that $g\widehat{t_1} = \Lambda^T \Lambda \widehat{t_1} = 0$. Thus one of the eigenvectors of g is $\widehat{t_1}$ with the eigenvalue $\lambda_{t_1} = 0$, implying $\det(\Lambda) = 0$. Because g is a symmetrical matrix, the other two eigenvectors denoted by $\widehat{a}$ and $\widehat{b}$ should be orthogonal to each other and in the $n - t_2$ plane. The corresponding eigenvalues are denoted by λ_a and λ_b, respectively, with

$$\lambda_a \lambda_b = |\widehat{n} \times \widehat{s}|^2 |\widehat{F} \times \widehat{B}|^2, \tag{27}$$

where $\widehat{F} = F_1\widehat{x} + F_2\widehat{y} + F_3\widehat{z}$, $\widehat{B} = B_1\widehat{x} + B_2\widehat{y} + B_3\widehat{z}$.

Since $\lambda_{t_1}\lambda_a\lambda_b = \det(g) = \det(\Lambda)^2$, $\lambda_{t_1} = \det(\Lambda)^2/(\lambda_a\lambda_b)$. By observing Equation (12), we obtain $g\widehat{\overline{\overline{\varepsilon}}} = g\widehat{\overline{\overline{\mu}}} = \det(\Lambda)$. Therefore, $\widehat{\overline{\overline{\varepsilon}}}$ and $\widehat{\overline{\overline{\mu}}}$ can be expressed as

$$\widehat{\overline{\overline{\varepsilon}}} = \widehat{\overline{\overline{\mu}}} = \mathrm{diag}[\lambda_a\lambda_b/\det(\Lambda), \det(\Lambda)/\lambda_a, \det(\Lambda)/\lambda_b], \tag{28}$$

Author's personal copy

where the diagonal elements correspond to the principle axes $\widehat{t_1}$, $\widehat{a}$, and $\widehat{b}$, respectively. Since $\det(\Lambda) = 0$, we have $\epsilon_a = \mu_a = \epsilon_b = \mu_b = 0$, indicating that the cloak medium at S_2 is isotropic in the $n - t_2$ plane. Therefore, $\widehat{n}$ and $\widehat{t_2}$ can also be considered as the principle axes with $\epsilon_n = \mu_n = \epsilon_{t_2} = \mu_{t_2} = 0$. It is seen that ϵ_{t_1} and μ_{t_1} have infinitely large values. Thus, the inner boundary operates similarly to a combination of a PEC (perfect electric conductor) and a PMC (perfect magnetic conductor), which can support both electric and magnetic surface displacement currents in the t_1 direction (Zhang, Chen, Wu, Luo, Ran and Kong, 2007; Greenleaf, Kurylev, Lassas and Uhlmann, 2007c,b). In order to have zero reflection at S_2, the boundary conditions at this PEC and PMC combined layer require that the incident electric (magnetic) fields in the t_1 direction and normal electric (magnetic) displacement fields are all zero. From Equation (21), we have $\widehat{E}^i_{t_1} = \widehat{H}^i_{t_1} = 0$. Since $\epsilon_n = \mu_n = 0$, we obtain $\widehat{D}^i_n = \widehat{B}^i_n = 0$. Therefore, it is proved that no reflection is excited at S_2, and $\widehat{\mathbf{E}}^i$ and $\widehat{\mathbf{H}}^i$ expressed in Equation (13) are just the total fields in the cloak medium. The PEC and PMC combined layer guarantees that no field can penetrate into the cloaked region. It is worth noting that the induced displacement surface currents in the t_1 direction make $\widehat{E}^i_{t_2}$ and $\widehat{H}^i_{t_2}$ at S_2 go down to zero. However, $\widehat{E}^i_{t_2}$ and $\widehat{H}^i_{t_2}$ are not zero at the location approaching S_2 in the cloak medium and thus are discontinuous across the inner boundary S_2 (Zhang, Chen, Wu, Luo, Ran and Kong, 2007; Greenleaf, Kurylev, Lassas and Uhlmann, 2007c,b).

4.2.2 Point-transformed Cloaks

In this case, a point with the coordinate $[c_1, c_2, c_3]$ maps to a closed surface S_2 as the cloak's inner boundary. At S_2, we have $f_1(q_1, q_2, q_3) = c_1$, $f_2(q_1, q_2, q_3) = c_2$, and $f_3(q_1, q_2, q_3) = c_3$. The transmitted electric and magnetic fields at the inner boundary can be decomposed into $\widehat{\mathbf{E}}^i = [\widehat{E}^i_n, \widehat{E}^i_{t_1}, \widehat{E}^i_{t_2}]$ and $\widehat{\mathbf{H}}^i = [\widehat{H}^i_n, \widehat{H}^i_{t_1}, \widehat{H}^i_{t_2}]$, where the definition of the subscript "n" denotes the normal direction of S_2, which is outward from the cloaked region; "t_1" and "t_2" represent the two tangential directions of S_2, which are perpendicular to each other, as shown in Figure 3(b). Consider Λ^T at the inner boundary, which can be expressed as

$$\Lambda^T = \mathrm{diag}[F_1\widehat{n}, F_2\widehat{n}, F_3\widehat{n}], \tag{29}$$

with

$$|F_i| = \sqrt{(\partial f_i/\partial q_1)^2 + (\partial f_i/\partial q_2)^2 + (\partial f_i/\partial q_3)^2}, \tag{30}$$

Author's personal copy

where $i = 1, 2, 3$. Then considering Equation (29), it can be derived that at S_2

$$\widehat{E}^i_{t_1} = \widehat{H}^i_{t_1} = 0, \tag{31}$$

$$\widehat{E}^i_{t_2} = \widehat{H}^i_{t_2} = 0, \tag{32}$$

$$\widehat{E}^i_n = [F_1, F_2, F_3]\mathbf{E}^i, \quad \widehat{H}^i_n = [F_1, F_2, F_3]\mathbf{H}^i. \tag{33}$$

Unlike the line-transformed cloak, in this case the tangential fields are all zero, implying that no field discontinuity exists at S_2.

Analyzing g similarly, as in the line-transformed cloak case, we obtain that $\widehat{n}$ is an eigenvector of g with the eigenvalue $\lambda_n = F_1^2 + F_2^2 + F_3^2$. While the other two eigenvectors are $\widehat{t_1}$ and $\widehat{t_2}$ with corresponding eigenvalues $\lambda_{t1} = \lambda_{t2} = 0$. This indicates that $\det(\Lambda) = 0$. Considering $\lambda_n\lambda_{t1}\lambda_{t2} = \det(\Lambda)^2$, we have $\lambda_{t1} = \lambda_{t2} = \det(\Lambda)/\sqrt{(F_1^2 + F_2^2 + F_3^2)}$. Therefore, $\widehat{\overline{\varepsilon}}$ and $\widehat{\overline{\mu}}$ are given as

$$\widehat{\overline{\varepsilon}} = \widehat{\overline{\mu}} = \mathrm{diag}[\det(\Lambda)^2/(F_1^2 + F^2 + F^3), \sqrt{F_1^2 + F^2 + F^3}, \sqrt{F_1^2 + F^2 + F^3}], \tag{34}$$

where the diagonal elements are in the principle axes $\widehat{n}$, $\widehat{t_1}$, and $\widehat{t_2}$, respectively. Since $\det(\Lambda) = 0$, $\epsilon_n = \mu_n = 0$. Considering $\epsilon_n = \mu_n = 0$, and that the tangential components of the incident fields at S_2 are zero, we conclude that no reflection is excited at S_2, and no field can penetrate into the cloaked region. The fields expressed in Equation (13) are the total fields in the cloak medium.

In this section, it has been proved that no reflection is excited at either the outer or the inner boundaries of an arbitrarily shaped cloak, and no field can penetrate into the cloaked region. Therefore, invisibility cloaks of arbitrary shape constructed by general coordinate transformations are confirmed.

5. CYLINDRICAL INVISIBILITY CLOAK

In this section, we will comprehensively study the performance of cylindrical invisibility cloaks, including both ideal ones and those with simplified material parameters. The cylindrical form is by far the most extensively studied invisibility cloaking structure. Some previous studies include Cummer, Popa, Schurig, Smith and Pendry (2006), Schurig, Mock, Justice, Cummer, Pendry, Starr and Smith (2006a), Cai, Chettiar, Kildishev and Shalaev (2007a), Ruan, Yan, Neff and Qiu (2007), Yan, Ruan and Qiu

Author's personal copy

(2007a), Greenleaf, Kurylev, Lassas and Uhlmann (2007c), Yan, Ruan and Qiu (2007b), Zhang, Chen, Wu, Luo, Ran and Kong (2007), Cai, Chettiar, Kildishev, Shalaev and Milton (2007b), Yan, Yan, Ruan and Qiu (2008d,c).

A cylindrical cloak is in fact a special type of line-transformed cloak. It is constructed by compressing EM fields in a cylindrical region $r' < b$ into a concentric cylindrical shell $a < r < b$. Its inner boundary is blown up by a straight line. Here we consider a generalized coordinate transformation in cylindrical coordinates in which $r' = f(r)$ with $f(a) = 0$ and $f(b) = b$, while θ and z are kept unchanged. The permittivity and permeability of the cloak expressed in the cylindrical coordinate system are as follows

$$\epsilon_r = \mu_r = \frac{f(r)}{rf'(r)}, \quad \epsilon_\theta = \mu_\theta = \frac{rf'(r)}{f(r)}, \quad \epsilon_z = \mu_z = \frac{f(r)f'(r)}{r}, \tag{35}$$

where the superscript $'$ denotes differentiation.

Consider the fields $\mathbf{E}^i$ and $\mathbf{H}^i$ incident upon the cloak. The fields in the cloaked medium can be obtained directly from Equation (13)

$$\widehat{E}_r(r,\theta,z) = f'(r)E_r^i(f(r),\theta,z), \quad \widehat{H}_r(r,\theta,z) = f'(r)H_r^i(f(r),\theta,z), \tag{36}$$

$$\widehat{E}_\theta(r,\theta,z) = \frac{f(r)}{r}E_\theta^i(f(r),\theta,z), \quad \widehat{H}_\theta(r,\theta,z) = \frac{f(r)}{r}H_\theta^i(f(r),\theta,z), \tag{37}$$

$$\widehat{E}_z(r,\theta,z) = E_z^i(f(r),\theta,z), \quad \widehat{H}_z(r,\theta,z) = H_z^i(f(r),\theta,z), \tag{38}$$

where $[E_r^i, E_\theta^i, E_z^i]$ and $[H_r^i, H_\theta^i, H_z^i]$ are components of the incident fields expressed in cylindrical coordinate form.

At the inner boundary, one can easily see that, no matter what $f(r)$ is, ϵ_θ and μ_θ are infinitely large, and the other components are zero, due to the fact that it is a line-transformed cloak. Field components E_θ and H_θ, D_r and B_r are all zero at the inner boundary $r = a$, which guarantees that no reflection is excited at the inner boundary, as analyzed above. The surface displacement currents are induced to make E_z and H_z tend to zero at the inner boundary (Zhang, Chen, Wu, Luo, Ran and Kong, 2007; Greenleaf, Kurylev, Lassas and Uhlmann, 2007c,b).

By choosing different radial mapping functions, we can obtain different parameters for the cloak medium. One possible class of functions can take the form of

$$r' = \frac{b}{(b-a)^n}(r-a)^n, \tag{39}$$

Author's personal copy

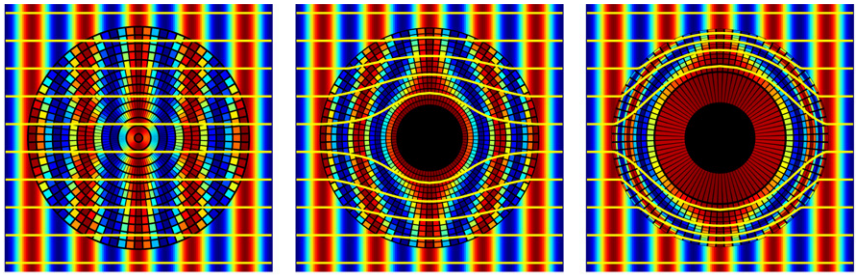

FIGURE 4 E_z field distributions in $r\theta$ plane. (a) Virtual EM space; (b) Cloak with $n = 1$; (c) Cloak with $n = 3$. Colormap: E_z. Green lines: Poynting vectors. Invariant coordinate lines are imposed. (For interpretation of the references to colour in this figure legend, the reader is referred to the web version of this article.)

where n is the transformation order. The corresponding parameters of the cloaks are

$$\varepsilon_r = \mu_r = \frac{r-a}{nr}, \quad \varepsilon_\theta = \mu_\theta = \frac{nr}{r-a}, \quad \varepsilon_z = \mu_z = \frac{nb^2(r-a)^{2n-1}}{(b-a)^{2n}r}. \tag{40}$$

When $n = 1$, it is the well-known linear cylindrical cloak as proposed by Schurig, Mock, Justice, Cummer, Pendry, Starr and Smith (2006a). The interactions between an in-plane propagating plane wave with E_z polarization and cylindrical cloaks designed with different n are shown in Figure 4. Figure 4(a) shows a plane wave propagating in the original free EM space. Figure 4(b) and (c) show interactions of the plane wave with two cloaks, designed with $n = 1$ and $n = 3$, respectively. Comparing Figure 4(b) and (c), we see that the Poynting vectors (rays) are bent much more heavily in the cloak medium when $n = 3$ than when $n = 1$.

As mentioned earlier, the inner boundary of a cylindrical cloak is inherently singular, i.e., the components of the permittivity and permeability in the θ direction are infinitely large, which are impossible to obtain in reality. To avoid this, there are two approaches: one is to remove a thin layer from the inner boundary, i.e., to construct an approximate ideal cloak; the other is to simplify the parameters of an ideal cloak, which not only circumvents the singular inner surface problem, but also makes implementation much easier. However, such material simplification is done at the expense of degradation of invisibility performance, owing to a change in the wave equation. In the following, we will first examine the properties of an approximate ideal cloak, then some material simplification methods will be summarized and compared.

Author's personal copy

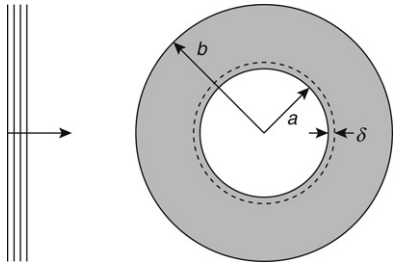

FIGURE 5 The schematic of a near-ideal cylindrical cloak: The distribution of the material parameter is the same as the ideal one shown in Equation (35), and the outer boundary is still fixed at $r = b$. However, the actual inner boundary is at $r = a + \delta$, where δ is a very small positive number

5.1 Approximate Ideal Cylindrical Cloak

The material parameters for a general radially transformed cylindrical cloak are derived in Equation (35). To avoid divergence at the inner boundary $r = a$, a thin layer is removed from the inner boundary, as illustrated in Figure 5. The goal here is to find the scattering performance of such an approximate cylindrical cloak. Without loss of generality, here we focus on the TM polarization (the magnetic field of the wave is polarized purely along the z axis). The relevant material parameters are therefore only μ_z, ϵ_r and ϵ_θ. Throughout the following discussion, the time dependence $\mathrm{e}^{-\mathrm{i}\omega t}$ is assumed.

As shown in Equation (8), the eigenfunction of the wave equations in the cloak is related to the eigenfunction in free space by the matrix Λ^T. Thus, the general form of the H_z component outside the cloak and in the cloak medium can always be expressed as

$$H_z = \sum_{n=-\infty}^{+\infty} a_n^{in} J_n(k_0 r)\mathrm{e}^{\mathrm{i}n\theta} + a_n^{sc} H_n(k_0 r)\mathrm{e}^{\mathrm{i}n\theta} \quad (b < r), \tag{41}$$

$$H_z = \sum_{n=-\infty}^{+\infty} a_n^{1} J_n(k_0 f(r))\mathrm{e}^{\mathrm{i}n\theta} + a_n^{2} H_n(k_0 f(r))\mathrm{e}^{\mathrm{i}n\theta} \quad (a + \delta < r < b). \tag{42}$$

In Equations (41) and (42), J_n and H_n represent Bessel functions of the first kind and Hankel functions of the first kind, respectively, both of the order n; a_n^{in} and a_n^{sc} are the expansion coefficients for the incident and scattered fields outside the cloak, respectively; a_n^i $(i = 1, 2)$ are the expansion coefficients for the field in the cloak shell; and $k_0 = \omega/c$ is the wavenumber in free space. H_z and E_θ in the region $r < a + \delta$ can be

Author's personal copy

expressed as

$$H_z = \sum_n a_n^3 S_n(r) \mathrm{e}^{\mathrm{i}n\theta}, \tag{43}$$

$$E_\theta = \sum_n k_0 a_n^3 T_n(r) \mathrm{e}^{\mathrm{i}n\theta}/(\mathrm{i}\omega\epsilon_0), \tag{44}$$

respectively, where ϵ_0 is the permittivity of the free space, and $S_n(r)$ and $T_n(r)$ are determined by the media in the cloaked region. For isotropic homogeneous media with relative permittivity ϵ_u and permeability μ_u, $S_n(r) = J_n(k_u r)$ and $T_n(r) = J_n'(k_u r)\sqrt{\mu_u/\epsilon_u}$, where $k_u = \omega\sqrt{\mu_u\epsilon_u}/c$. However, when the cloaked region is composed of inhomogeneous or anisotropic media, close forms of $S_n(r)$ and $T_n(r)$ are difficult to obtain.

The boundary conditions require that tangential fields should be continuous across the interfaces at $r = b$ and $r = a + \delta$. The boundary conditions lead to the set of equations:

$$a_n^{in} J_n(k_0 b) + a_n^{sc} H_n(k_0 b) = a_n^1 J_n(k_0 b) + a_n^2 H_n(k_0 b), \tag{45}$$

$$k_0 a_n^{in} J_n'(k_0 b) + k_0 a_n^{sc} H_n'(k_0 b) = \frac{f'(b)k_0}{\epsilon_\theta(b)} a_n^1 J_n'(k_0 b) + \frac{f'(b)k_0}{\epsilon_\theta(b)} a_n^2 H_n'(k_0 b), \tag{46}$$

$$a_n^1 J_n(k_0 f(a+\delta)) + a_n^2 H_n(k_0 f(a+\delta)) = a_n^3 S_n(a+\delta), \tag{47}$$

$$\frac{f'(a+\delta)k_0}{\epsilon_\theta(a+\delta)} a_n^1 J_n'(k_0 f(a+\delta)) + \frac{f'(a+\delta)k_0}{\epsilon_\theta(a+\delta)} a_n^2 H_n'(k_0 f(a+\delta)) = k_0 a_n^3 T_n(a+\delta), \tag{48}$$

From Equations (45)–(48), one can easily obtain the expression of the scattering coefficient for each order, which is defined as $C_n^{sc} = a_n^{sc}/a_n^{in}$. It can be proved that $C_n^{sc} \to 0$ when $\delta \to 0$ (see Ruan, Yan, Neff and Qiu (2007) in the case of a linearly tranformed cloak). That is, the ideal cylindrical cloak is a perfect invisibility cloak for generalized coordinate transformations. Here we pay particular attention to the effect of a tiny perturbation δ. We notice that, when $\delta \ll a$ and $k_0\delta \ll 1$, C_n^{sc} can be approximated as

$$C_n^{sc} \approx \frac{a J_n(k_0\delta_f) T_n(a+\delta) - \delta_f J_n'(k_0\delta_f) S_n(a+\delta)}{\delta_f H_n'(k_0\delta_f) S_n(a+\delta) - a H_n(k_0\delta_f) T_n(a+\delta)}, \tag{49}$$

where $\delta_f = f^p(a)\delta^p$, $f^p(a) = \mathrm{d}^p f(r)/\mathrm{d}r^p|_{r=a}$, with $p \geq 1$ and $f^q(a) = 0$ for $q < p$. For the special case when a PEC layer or a PMC layer is put at

Author's personal copy

$r = a+\delta$, Equation (49) is still valid by setting $S_n(a+\delta) = 1$ and $T(a+\delta) = 0$ for the PEC case, or setting $S_n(a+\delta) = 0$ and $T(a+\delta) = 1$ for the PMC case.

In the following, based on the scattering equation given in Equation (49), we will show that the zeroth order scattering term is very sensitive to the perturbation, while the high order scattering terms are not so sensitive. A method is then proposed to overcome the high sensitivity problem for the zeroth order wave.

5.1.1 zeroth Order Scattering Coefficient

For the zeroth order term, since $J_0' = -J_1$ and $H_0' = -H_1$, we obtain

$$C_0^{sc} \approx \frac{aJ_0(k_0\delta_f)T_0(a+\delta) + \delta_f J_1(k_0\delta_f)S_0(a+\delta)}{-\delta_f H_1(k_0\delta_f)S_0(a+\delta) - aH_0(k_0\delta_f)T_0(a+\delta)}. \tag{50}$$

Considering the asymptotic forms of the Bessel functions, we have $J_0(k_0\delta_f) \approx 1$ and $\delta_f J_1(k_0\delta_f) \approx k_0\delta_f^2/2$. Therefore we know that the numerator of Equation (50) will be dominated by $aJ_0(k_0\delta_f)T_0(a+\delta)$ except for the case where a PEC layer is put at the cloak's inner surface and $T_0(a+\delta)$ is always equal to zero. In view of this, we will present, separately, the following two different cases: (1) no PEC layer is at $r = a+\delta$ and (2) there is a PEC layer at $r = a+\delta$.

Case (1): no PEC layer at $r = a+\delta$

In this case, the numerator of Equation (50) will be dominated by $aJ_0(k_0\delta_f)T_0(a+\delta)$, so C_0^{sc} can be further simplified to

$$C_0^{sc} \approx \frac{aJ_0(k_0\delta_f)T_0(a+\delta)}{\mathrm{i}2S_0(a+\delta)/(\pi k_0) - aH_0(k_0\delta_f)T_0(a+\delta)}, \tag{51}$$

where $\delta_f H_1(k_0\delta_f) \approx -\mathrm{i}2/(\pi k_0)$ is considered. To verify the validity of Equation (51), we take an example with $f(r) = b(r-a)/(b-a)$, $a = 1.2\pi/k_0$, $b = 2\pi/k_0$, and the region inside the cloak shell being air. Using Equation (51), $|C_0^{sc}|$ versus δ for small values of δ is plotted in Figure 6. It is seen that the result calculated from Equation (51) fits very well with the exact result obtained directly from Equations (45)–(48).

Observing Equation (51) and noting that $H_0(k_0\delta_f)$ diverges with the decrease of δ, we find that the value of C_0^{sc} can be approximated by $J_0(k_0\delta_f)/H_0(k_0\delta_f) \propto -1/\ln(\delta)$, which is independent of the media inside the cloak, under the circumstance that no PEC layer is at the inner boundary. This results in a very slow convergence rate for C_0^{sc}, approaching zero as δ decreases (also see Ruan, Yan, Neff and Qiu (2007)). Thus, C_0^{sc} is sensitive to perturbation in this case. In other words, a

Author's personal copy

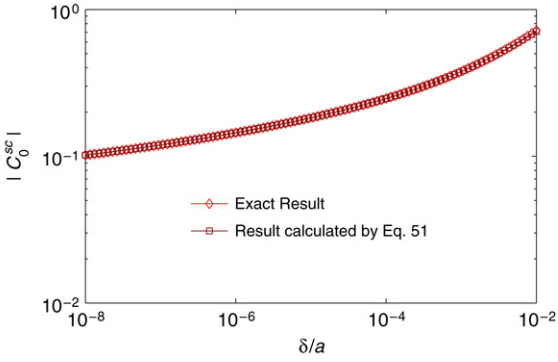

FIGURE 6 $|C_0^{sc}|$ versus δ for a cylindrical cloak with $f(r) = b(r-a)/(b-a)$, $a = 1.2\pi/k_0$, $b = 2\pi/k_0$, and the region inside the cloak shell is assumed to be air

noticeable scattering will be induced even by a tiny perturbation, for example, from Figure 6, $|C_0^{sc}|$ is 0.1017 even when $\delta/a = 10^{-8}$.

However, by choosing an appropriate $f(r)$, the noticeable scattering induced by a tiny perturbation can be reduced to some extent. Observing Equation (51), we find that $|C_0^{sc}|$ decreases when δ_f decreases. Since $\delta_f = f^p(a)\delta^p$, we know that by choosing an $f(r)$ with a small $f^p(a)$ and a large p we can reduce the scattering coefficient. To verify this idea, the zeroth order scattering coefficients are derived for three types of cylindrical cloaks. The parameters a, b, and the medium inside the cloak shell are kept the same as in Figure 6. $k_0 = 0.064/\pi$. The function $f(r)$ is chosen consecutively for three case studies as $f(r) = b(r-a)/(b-a)$ with $p = 1$ and $f'(a) = 2.5$, $f(r) = b(r^{10} - a^{10})/(b^{10} - a^{10})$ with $p = 1$ and $f'(a) = 0.1$, and $f(r) = b/2 - b/2\cos(\pi/(b-a)(x-a))$ with $p = 2$ and $f''(a) = 0.1$. $|C_0^{sc}|$ versus δ for three cloaks are plotted in Figure 7. It is seen that $|C_0^{sc}|$ decreases with the decrease of $f'(a)$ and the increase of p. However the reduction in the scattering coefficient is not significant because the overall convergence speed determined by $-1/\ln(\delta)$ can not be improved.

Case (2): with a PEC layer at $r = a + \delta$

When a PEC layer is present, Equation (51) can be simplified to

$$C_0^{sc} = -\frac{J_1(k_0\delta_f)}{H_1(k_0\delta_f)}. \tag{52}$$

In Equation (52), the value of C_0^{sc} is determined by $J_1(k_0\delta_f)/H_1(k_0\delta_f) \propto \delta^{2p}$. δ^{2p} converges to zero much faster than $-1/\ln(\delta)$, therefore, in this case C_0^{sc} also converges to zero much faster, i.e., C_0^{sc} is not sensitive to

Author's personal copy

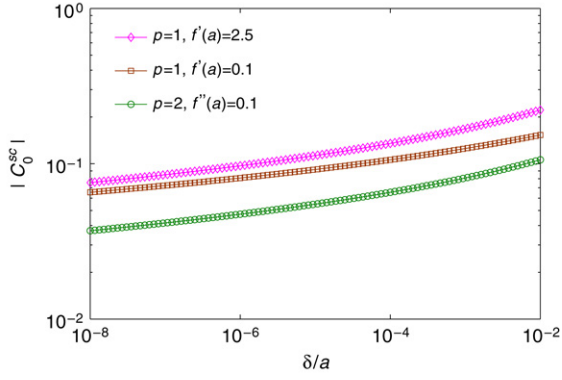

FIGURE 7 $|C_0^{sc}|$ versus δ for $p = 1$ and $f'(a) = 2.5$, $p = 1$ and $f'(a) = 0.1$, $p = 2$ and $f''(a) = 0.1$. Other parameters are the same as those in Figure 6

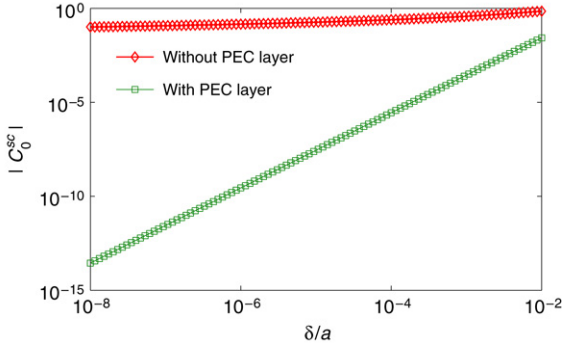

FIGURE 8 $|C_0^{sc}|$ versus δ for the case (1) without a PEC layer at $r = a + \delta$ and the case (2) with a PEC layer at $r = a + \delta$. Other parameters are the same as those in Figure 6

the perturbation. To show the improvement of the convergence speed of C_0^{sc}, we calculate $|C_0^{sc}|$ versus δ with $f(r) = b(r - a)/(b - a)$, $a = 1.2\pi/k_0$, $b = 2\pi/k_0$, for both case (1) and case (2). The region inside the cloak shell is air for case (1). The result is shown in Figure 8. It clearly indicates that the convergence speed of C_0^{sc} is improved drastically by introducing a PEC layer at $r = a + \delta$ (Yan, Yan, Ruan and Qiu, 2008d; Greenleaf, Kurylev, Lassas and Uhlmann, 2007c).

5.1.2 High Order Scattering Coefficients

For the high order terms, considering the asymptotic forms of the Bessel function and Hankel function for small arguments when $\delta_f J_n'(k_0\delta_f) \approx$

Author's personal copy

$|n|J_n(k_0\delta_f)/k_0$, and $\delta_f H_n'(k_0\delta_f) \approx -|n|H_n(k_0\delta_f)/k_0$, we arrive at

$$C_n^{sc} \approx -A_n B_n, \tag{53}$$

where

$$A_n = \frac{k_0 a T_n(a+\delta) - |n| S_n(a+\delta)}{k_0 a T_n(a+\delta) + |n| S_n(a+\delta)}, \quad B_n = \frac{J_n(k_0\delta_f)}{H_n(k_0\delta_f)}. \tag{54}$$

From Equation (54), it can be seen that A_n is nearly a constant, which characterizes the properties of the cloaked region. However, B_n is affected significantly by the perturbation. Therefore, the value of C_n^{sc} is mainly determined by B_n, i.e., $J_n(k_0\delta_f)/H_n(k_0\delta_f) \propto \delta^{2|n|p}$, which is, unlike the case for the zeroth order, independent of the situation whether a PEC layer is put at the inner boundary or not. To verify the validity of Equation (53), we take again the example with $f(r) = b(r-a)/(b-a)$, $a = 1.2\pi/k_0$, $a = 2\pi/k_0$, and the region inside the cloak shell being air. $|C_n^{sc}|$ for $n = 1$ and $n = 2$ when $10^{-8}a < \delta < 10^{-2}a$ are plotted in Figure 9(a) and (b), respectively. We see that the results calculated from Equation (53) agree with the exact results almost perfectly. In addition, by comparing Figures 6 and 9, it is obvious that the high order scattering coefficients converge much faster than the zeroth order coefficient. Interestingly, the convergence speed of C_1^{sc} determined by δ^{2p} is the same as that of C_0^{sc} if a PEC layer is put at $r = a + \delta$.

5.2 Material Simplification

To implement an ideal cylindrical invisibility cloak, two restrictions exist. One is that some material parameters require an infinitely large value at the inner boundary, and the other is that each anisotropic material parameter varies with its spatial location. The first restriction can be solved by removing a thin layer from the inner boundary, as mentioned in the above subsection. However, the existence of the second restriction still makes practical implementation difficult. Therefore, it is useful to simplify the material parameters of an ideal cylindrical invisibility cloak.

The first simplified model was proposed in Cummer, Popa, Schurig, Smith and Pendry (2006) and later demonstrated in Schurig, Mock, Justice, Cummer, Pendry, Starr and Smith (2006a). In these preliminary works, the radial transformation function is considered to be a linear function $r' = f(r) = b(r-a)/(b-a)$. The corresponding ideal material parameters and simplified material parameters are listed in Table 1. It is obvious that the implementation of such a cloak will become much easier after simplification: no material parameter requires an infinite value; and only ε_r and μ_r are inhomogeneous, while the other components

Author's personal copy

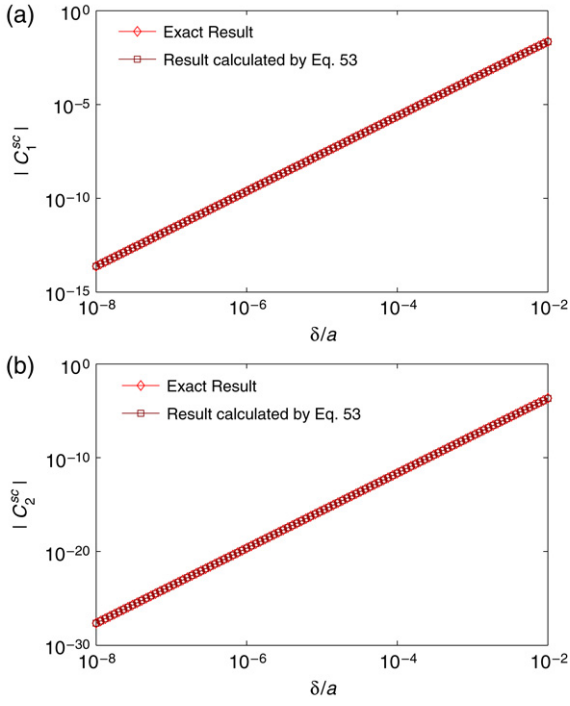

FIGURE 9 (a) $|C_1^{sc}|$ versus δ; (b) $|C_2^{sc}|$ versus δ. Other parameters are the same as those in Figure 5

TABLE 1 Material parameters for linear cloaks

Ideal	Simplified (Schurig, Mock, Justice, Cummer, Pendry, Starr and Smith, 2006a)
$\varepsilon_r = \mu_r = \frac{r-a}{r}$	$\varepsilon_r = \mu_r = \left(\frac{r-a}{r}\right)^2$
$\varepsilon_\theta = \mu_\theta = \frac{r}{r-a}$	$\varepsilon_\theta = \mu_\theta = 1$
$\varepsilon_z = \mu_z = \left(\frac{b}{b-a}\right)^2 \frac{r-a}{r}$	$\varepsilon_z = \mu_z = \left(\frac{b}{b-a}\right)^2$

are all constant. In the case where normal incidence (the **k** vector is perpendicular to the cloak cylinder axis) and single TE polarization (the electric field only exists in the z direction) are considered, we need only account for three material components, μ_r, μ_θ and ϵ_z. Among these three

Author's personal copy

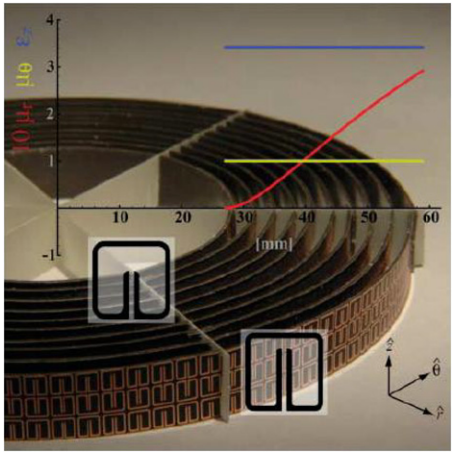

FIGURE 10 2D microwave cloaking structure (Schurig, Mock, Justice, Cummer, Pendry, Starr and Smith, 2006a)

parameters, we need only pay special attention to μ_r when it comes to engineering the necessary metamaterial. In Ref. (Schurig, Mock, Justice, Cummer, Pendry, Starr and Smith, 2006a), such a simplified cloak for TE polarization at microwave frequency is experimentally demonstrated. As shown in Figure 10, the native cylindrical coordinate has been used as the construction coordinate. The key component μ_r is engineered by a split ring resonator (SRR) structure, and its variation along the radial direction is achieved by tuning the geometrical parameters of the SRRs. The experimental results are shown in Figure 11.

Simplified cylindrical invisibility cloaks make the implementation much easier. However, this is at the expense of loss of the perfect invisibility performance, since the material parameters deviate from the ideal values. The arguments in Cummer, Popa, Schurig, Smith and Pendry (2006) and Schurig, Mock, Justice, Cummer, Pendry, Starr and Smith (2006a) are presented mostly through examining numerically simulated or experimentally recorded field distributions. The exact scattering induced by their simplified cloak model is not quantified. In the following, we will show a more precise quantitative analysis of simplified cloaks and show some optimal simplified models.

5.2.1 Simplified Linear Cloak

Consider a simplified cylindrical cloak with the material parameters listed in Table 1. Both domains inside and outside the cloak are assumed to be air. The structure is in general a three-layered cylindrical scatterer. We refer to the layers from inside to outside as layer 1, 2 and 3, respectively.

Author's personal copy

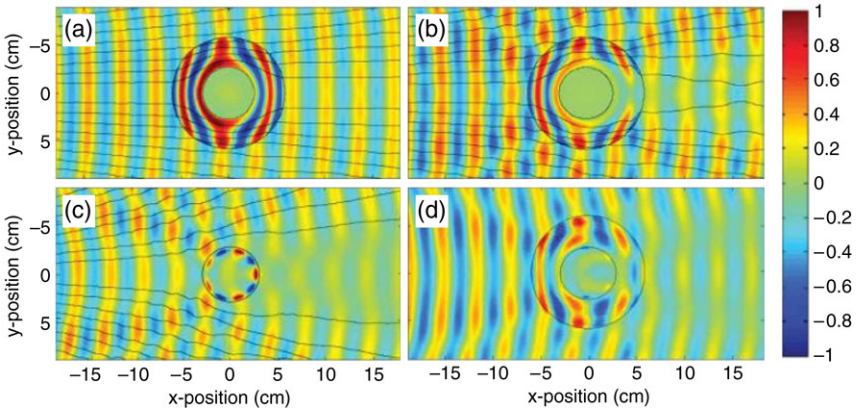

FIGURE 11 Snapshots of time-dependent, steady-state electric field patterns, with stream lines indicating the direction of power flow (i.e., the Poynting vector). The fields shown are (a) simulation of the cloak with the exact material properties, (b) simulation of the cloak with the reduced material properties, (c) experimental measurement of the bare conducting cylinder, and (d) experimental measurement of the cloaked conducting cylinder (Schurig, Mock, Justice, Cummer, Pendry, Starr and Smith, 2006a)

The analysis is on normal incidence with TE polarization. The TM polarization case can be easily derived by the duality principle. By default, we choose the cloak's cylindrical coordinate as the global coordinate. In a homogeneous material region (i.e. the cloak interior and exterior) the general solution is expressible in Bessel functions. Within the cloak medium, the general wave equation that governs the E_z field can be written as

$$\frac{1}{r}\left[\frac{\partial}{\partial r}\left(\frac{r}{\mu_\theta}\frac{\partial E_z}{\partial r}\right)\right]+\frac{1}{r^2}\frac{\partial}{\partial\theta}\left(\frac{1}{\mu_r}\frac{\partial E_z}{\partial\theta}\right)+k_0^2\varepsilon_z E_z=0. \tag{55}$$

In the case of the simplified cloak, the invariant μ_θ can be taken out of the differential operator in Equation (55). This is however not true for the ideal cloak medium. Therefore the wave behaviour within the cloak shell is altered when compared to that in an ideal cloak.

Since the material parameters of such simplified cloaks are azimuthally invariant (which is also true for the ideal parameter set), we can use the variable separation $E_z = \Psi(r)\Theta(\theta)$. Equation (55) can then be decomposed into

$$\frac{\mathrm{d}^2\Theta}{\mathrm{d}\theta^2}+m^2\Theta=0, \tag{56}$$

Author's personal copy

$$\frac{\mathrm{d}}{\mathrm{d}r}\left(\frac{r}{\mu_\theta}\frac{\mathrm{d}\Psi}{\mathrm{d}r}\right) + k_0^2 r\varepsilon_z\Psi - m^2\frac{1}{r\mu_r}\Psi = 0, \tag{57}$$

where m is an integer. The solution to Equation (56) is $\exp(\mathrm{i}m\theta)$. Equation (57) is a second-order homogeneous differential equation so two independent solutions are expected. At this moment, we assume the solution to Equation (57), for a fixed m, can be written in general as $\mathscr{A}_m Q_m + \mathscr{B}_m R_m$, where $\mathscr{A}_m$ and $\mathscr{B}_m$ are constants. Q_m and R_m are functions of r. Now valid field solutions in the three layers (denoted by superscripts) can be described by

$$E_z^1 = \sum_m \mathscr{A}_m^1 J_m(k_0 r)\exp(\mathrm{i}m\theta), \tag{58}$$

$$E_z^2 = \sum_m \{\mathscr{A}_m^2 Q_m + \mathscr{B}_m^2 R_m\}\exp(\mathrm{i}m\theta), \tag{59}$$

$$E_z^3 = \sum_m \{\mathscr{A}_m^3 J_m(k_0 r) + \mathscr{B}_m^3 H_m(k_0 r)\}\exp(\mathrm{i}m\theta). \tag{60}$$

H_m is the Hankel function, which represents an outward-travelling cylindrical wave. The J_m and H_m terms in the 3rd layer physically correspond to the incident and scattered waves, respectively. Hence, it is most important to solve the scattering problem, with $\mathscr{A}_m^1$ (transmitted field) and $\mathscr{B}_m^3$ (scattered field) subject to a given incidence $\mathscr{A}_m^3$.[2] Comparatively $\mathscr{A}_m^2$ and $\mathscr{B}_m^2$ are physically less interesting. The coefficients are solved by matching the tangential fields, E_z and H_θ, at the layer interfaces. Due to the orthogonality of the function $\exp(\mathrm{i}m\theta)$, the cylindrical waves in different orders decouple. Hence, we can examine the transmission and scattering of the cloak for each individual order number m.

By substituting the simplified material parameters into Equation (57), we obtain

$$(r-a)^2\frac{\mathrm{d}^2\Psi}{\mathrm{d}r^2} + \frac{(r-a)^2}{r}\frac{\mathrm{d}\Psi}{\mathrm{d}r} + \left[(r-a)^2\left(\frac{b}{b-a}\right)^2 k_0^2 - m^2\right]\Psi = 0. \tag{61}$$

Equation (61) has two non-essential singularities at $r = 0$ and $r = a$ for $m \neq 0$. It is worthwhile mentioning that, with the ideal parameters,

[2] For example, the right-travelling incidence plane wave $\exp(-\mathrm{j}k_0 x)$ can be expanded in Bessel functions, or a generalized Fourier series, as $\sum_m (-\mathrm{i})^m J_m(k_0 r)\exp(\mathrm{i}m\theta)$. Therefore $\mathscr{A}_m^3$ can be determined beforehand. See (Felbacq, Tayeb and Maystre, 1994).

Author's personal copy

Equation (61) can be written, instead, as

$$(r-a)^2\frac{\mathrm{d}^2\Psi}{\mathrm{d}r^2}+(r-a)\frac{\mathrm{d}\Psi}{\mathrm{d}r}+\left[(r-a)^2\left(\frac{b}{b-a}\right)^2k_0^2-m^2\right]\Psi=0. \quad (62)$$

When $m=0$, Equation (61) can be further simplified to

$$r^2\frac{\mathrm{d}^2\Psi}{dr^2}+r\frac{\mathrm{d}\Psi}{\mathrm{d}r}+r^2k_0^2\left(\frac{b}{b-a}\right)^2\Psi=0. \quad (63)$$

This is the zeroth-order Bessel differential equation. Its non-essential singularity remains at $r=0$. Equation (63) suggests that an incoming zeroth-order cylindrical wave would effectively see the simplified cloak as a homogeneous isotropic medium whose effective refractive index is $n_{\mathrm{eff}}=\frac{b}{b-a}$. Its transmission through the cloak shell is therefore determined by the etalon effect of the finite medium.

When $m\neq 0$, the wave solution is governed by Equation (61). In the following, the scattering coefficient s_m, subject to individual cylindrical wave incidences, will be derived. The scattering coefficient in each cylindrical order is defined as $s_m=\left|\mathscr{B}_m^3/\mathscr{A}_m^3\right|$. Analytic derivation of s_m can be done if two solutions to Equation (61) (i.e. Q_m and R_m) are known in closed form. However, despite its analogy to Equation (62), Equation (61) fails the analytic Frobenius method (Arfken, 1970). Here we tackle the problem by the finite-element method (FEM). The scattering problem is computed numerically. The field outside the cloak is then used for deriving coefficients $\mathscr{A}_m^3$ and $\mathscr{B}_m^3$ through a fitting procedure. s_m is known in turn. Solutions with different azimuthal orders are obtained by varying the azimuthal dependence of a circular current source outside the cloak. The scattering problem is numerically manageable since the functionals $\varepsilon_z\mu_\theta$ and $\frac{\mu_\theta}{\mu_r}$ in Equation (57), unlike in the ideal cloak case, are both finite and do not possess any removable singularity for the simplified medium. The commercial software COMSOL was deployed to carry out the calculations. In our case study, we fixed $a=0.1$ m and the operating frequency $f=2$ GHz. The performance of the cloak was examined as b was increased from 0.2 m. Similar parameters are also found in (Cummer, Popa, Schurig, Smith and Pendry, 2006).

The scattering coefficients in different azimuthal orders as a function of b are shown in Figure 12. As expected, the zeroth-order scattering coefficient is quite distinct from the others due to the different governing wave equation. In fact, an analytic solution exists when $m=0$. The excellent agreement between the numerical and analytic results for the zeroth-order scattering coefficient confirms the validity and accuracy of

Author's personal copy

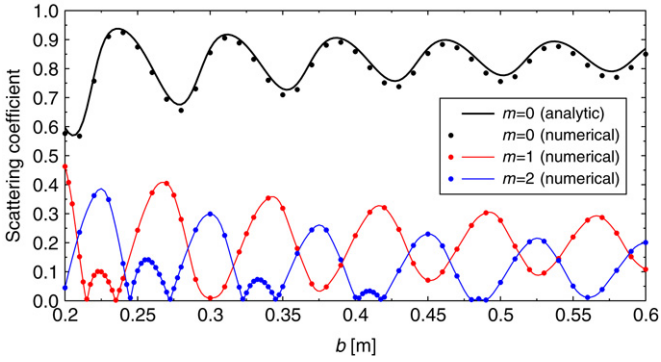

FIGURE 12 Variation of the scattering coefficients, examined in each cylindrical wave order, as a function of b. For $m = 1, 2$, the curves are fitted using the Savitzky-Golay smoothing filter according to numerically derived data points (dots)

our approach. It has been argued that the invisibility performance of a simplified cloak improves with increase of b. Here, using the analytic technique, the zeroth-order scattering coefficient is found to converge to 0.867 with respect to b. Despite the fact that the effective index of the cloak approaches 1 as b increases, the phase variation of the zeroth-order wave within the cloak medium is increasing, as $k_0 \frac{b}{b-a}(b-a) = k_0 b$. This explains why the scattering coefficient converges to a value other than 0. The existence of the zeroth-order scattering coefficient effectively disqualifies the cloak from being completely invisible.

Compared to the zeroth-order scattering coefficient, the high-order scattering coefficients (only those for $m = 1, 2$ are shown in Figure 12) are seen to behave in a similar oscillatory fashion, but in general are much smaller. The scattering coefficient tends to converge to a value closer to zero when the order number m increases. We should attribute the relatively small high-order scattering coefficients to the cloak's partial relation to the ideal cloak based on coordinate transformation. Having said that, however, our numerical result shows that the high-order scattering coefficients do not converge to zero even when the cloak wall is very thick. For comparison purposes, it should be mentioned that the scattering coefficient in any order of an annular cylinder varies between 0 and 1 as a function of either its refractive index (as the geometry is fixed) or its outer radius (as the material and inner radius are fixed).

Besides the requirement of zero scattering (invisibility), a device also needs to possess a spatial region which is in complete EM isolation from the outer world in order to be an invisibility cloak. Therefore it is meaningful to know how much the field penetrates into the simplified cloak, subject to a foreign EM illumination. Again, the problem is studied

Author's personal copy

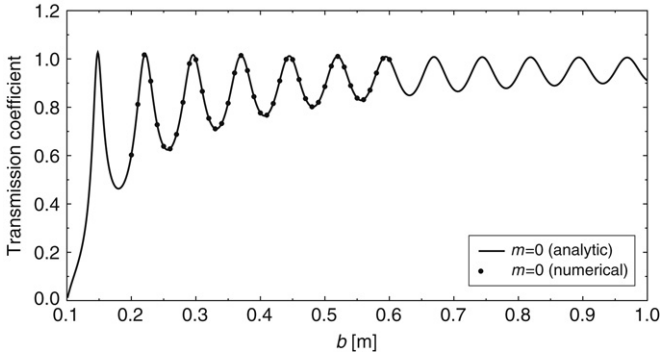

FIGURE 13 The zeroth-order transmission coefficient

by examining the individual cylindrical wave components separately. The transmission coefficient, defined as $t_m = \left|\mathscr{A}_m^1/\mathscr{A}_m^3\right|$, is used to characterize the field transmission. When $m = 0$, the amount of field transmitted into the cloak interior can be analytically derived, this is shown in Figure 13 as a function of b. The transmission is seen to be oscillatory, and converging to 1 as b increases. Numerical calculation is also superimposed for validation. When $m \neq 0$, the FEM calculations show that the field inside the cloak is almost zero. The corresponding transmission coefficients are exclusively smaller than 0.005 and hence are not plotted in Figure 13. This indicates that the contour $r = a$ provides an insulation between its enclosed domain and the outer domain, but only for all high-order cylindrical waves. Therefore, any objects placed inside the cloak are exposed to the zeroth-order cylindrical wave component. Conversely, the zeroth-order wave component of an EM source placed within the cloak (or a wave scattered by objects inside the cloak) will transmit out. As a result, objects enclosed by a simplified cloak may be sensed by a foreign detection unit.

5.2.2 Optimal Models of Simplified Cloaks

For the simplified cloak presented above, the material parameters, as listed in Table 1, do not satisfy the perfectly-matched layer (PML) condition at the outer interface. The reflective outer interface becomes a factor causing scattering. One can see that, to keep the functionals $\mu_\theta \varepsilon_z$ and $\mu_r \varepsilon_z$ invariant with respect to the ideal values, more than one solution exists. Here, we show another set of material parameters of a simplified linear transformed cloak,

$$\epsilon_r = \mu_r = (\frac{r-a}{r})^2 \frac{b}{b-a}, \quad \epsilon_\theta = \mu_\theta = \frac{b}{b-a}, \quad \epsilon_z = \mu_z = \frac{b}{b-a}. \quad (64)$$

Author's personal copy

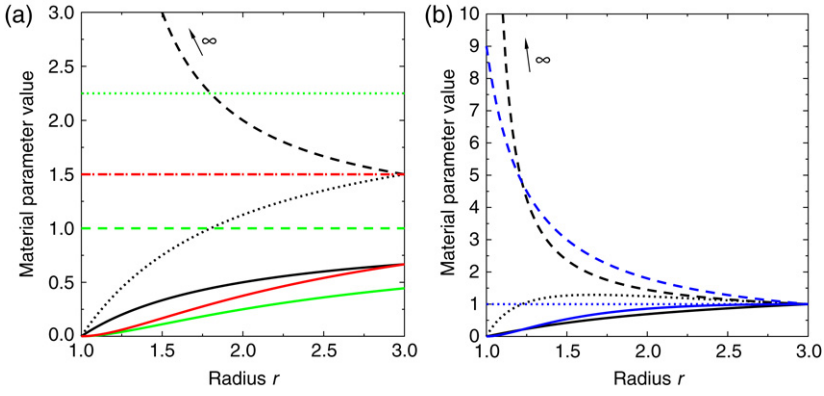

FIGURE 14 (a) Material parameters for an ideal linear cloak (black curves), a simplified linear cloak (green curves), and an improved linear cloak (red curves). (b) Material parameters for an ideal quadratic cloak (black curves), and an simplified quadratic cloak (blue curves). Solid line: μ_r; dashed line: μ_θ; dotted line: ε_z. All cloaks have $a = 1$ and $b = 3$ (a.u.)

For the new parameter set, at $r = b$, we have $\varepsilon_z = \mu_\theta = 1/\mu_r = b/(b-a)$, i.e. the PML condition. Therefore, with the impedance-matched outer surface, it is expected that a cloak with the new set of parameters would induce smaller scattering. The improved parameters are plotted in Figure 14(a) in red curves. Notice the unchanged material values at $r = b$ as compared to those for the ideal cloak (black curves).

The quadratic coordinate transformation was also proposed for the cloak design (Cai, Chettiar, Kildishev, Shalaev and Milton, 2007b). It is found that the simplified version of the quadratic cloak also matches the outer free space in impedance. The quadratic coordinate transformation takes the form

$$r = \left[\frac{b-a}{b} + p(r'-b)\right] r' + a, \tag{65}$$

where p can be arbitrary as long as $|p| < (b-a)/b^2$ is valid for keeping the spatial mapping monotonic. The ideal material parameters, according to such a coordinate transformation, are shown in the lefthand column of Table 2. Since p is free to change here, the material parameters can be varied. Interestingly, at $p = a/b^2$, we have $\frac{\mathrm{d}r}{\mathrm{d}r'}|_{r=b} = 1$. Under this condition, the material parameters are all valued at 1 at $r = b$. Electromagnetically, the resulting cloak does not even have an interface at $r = b$, i.e., the material parameters are the same as in free space. The anisotropic ratio of the cloak material then grows at radial positions

Author's personal copy

TABLE 2 Material parameters for quadratic cloaks

Ideal	Simplified (Cai, Chettiar, Kildishev, Shalaev and Milton, 2007b)
$\varepsilon_r = \mu_r = \frac{r'}{r}\left[p(2r'-b) + \frac{b-a}{b}\right]$	$\varepsilon_r = \mu_r = \left(\frac{r'}{r}\right)^2$
$\varepsilon_\theta = \mu_\theta = \frac{1}{\varepsilon_r}$	$\varepsilon_\theta = \mu_\theta = \frac{1}{\left[p(2r'-b)+\frac{b-a}{b}\right]^2}$
$\varepsilon_z = \mu_z = \frac{r'}{r}\frac{1}{p(2r'-b)+\frac{b-a}{b}}$	$\varepsilon_z = \mu_z = 1$

closer to the cloak's inner surface. Notice this particular choice of p value, together with the monotonicity condition, imposes a constraint on the *ideal* cloak's wall thickness, which is $b > 2a$. The material parameters for a sample ideal cloak are plotted in Figure 14(b) (black curves). Again a divergent μ_θ is observed at $r = a$. The cloak can also be simplified by keeping the functionals $\mu_\theta \varepsilon_z$ and $\mu_r \varepsilon_z$ invariant. The simplified cloak has the material parameters as given in the righthand column of Table 2. The simplified material parameters are plotted in Figure 14(b) (also with $p = a/b^2$). Notice that the "interfaceless" property at $r = b$ is inherited by the simplified cloak.

In the following, a detailed analysis of the above two optimal models of simplified cloaks will be given. Similar to the previous analysis, normal incidence and TE polarization are considered. As shown above, a simplified cloak allows a certain percentage of a foreign field to penetrate into the cylindrical shell. A quick and reliable fix to this problem is to introduce a PEC lining on the inner surface of the cloak shell. It follows that the invisibility performance is only characterized by the scattering induced by the cloak.

Three types of cylindrical cloaks, including the previously proposed simplified linear cloak (in Table 1), improved simplified linear cloak (Equation (64)), and the simplified quadratic cloak (Table 2) are presented here. All cloaks consist of a PEC lining. We examine their invisibility performance as a function of parameters a, b and λ. When the effect of b is analyzed, we fix $a = 0.1$ m and $\lambda = 0.15$ m (or $f = 2$ GHz). When the effect of a is analyzed, we fix $b = 0.6$ m and the frequency is unchanged. When the the effect of λ is analyzed, we fix $a = 0.2$ m and $b = 0.6$ m. The calculated scattering coefficients for the three types of simplified cloak are summarized in Figure 15. Panels in each row in Figure 15 are for a particular type of cloak, while panels in each column are for the effect of a particular parameter. Only the scattering coefficients for the first four

Author's personal copy

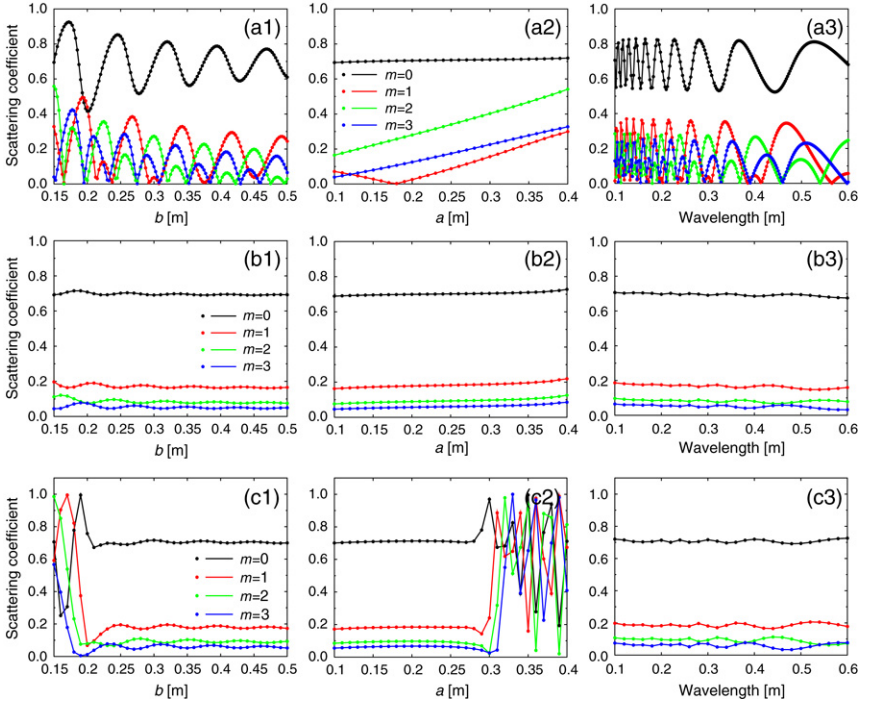

FIGURE 15 The scattering coefficients in each cylindrical order as a function of either b, a or λ. (a1)–(a3) Previously proposed simplified linear cloak; (b1)-(b3) Improved simplified linear cloak; (c1)–(c3) Simplified quadratic cloak. In each row, the left panel shows the effect of b as $a = 0.1$ m and $\lambda = 0.15$ m; the middle panel shows the effect of a as $b = 0.6$ m and $\lambda = 0.15$ m; the right panel shows the effect of λ as $a = 0.2$ m and $b = 0.6$ m.

cylindrical orders are presented. In general, for all cloaks the scattering is smaller when the order number m is larger.

From Figure 15, it is quite evident that the originally proposed simplified linear cloak [Figure 15(a1)–(a3)] induces relatively larger scattering in all cylindrical orders compared to the other two cloaks. The scattering in each order varies greatly as a, b or λ changes, suggesting the relatively strong cavity effect of the cloak. In a dramatic contrast, the scattering caused by the improved linear cloak [Figure 15(b1–b3)] has only a very slight dependence on either a, b or λ. The geometry-insensitive scattering characteristics should be attributed to the perfect impedance matching at the cloak's outer surface. The EM system now does not have a closed region bounded by reflective interfaces, therefore a cavity can't be formed. For the simplified quadratic cloak [Figure 15(c1–c3)], the scattering characteristics are quite similar to those of the improved linear

Author's personal copy

cloak when its geometry fulfills the $b > 2a$ condition. The relatively small scattering is again due to the outer surface being matched with the outer space. With a relatively thin cloak wall ($b < 2a$), incoming cylindrical waves, in general, experience heavy scattering. This result confirms the minimum thickness restriction, i.e. $b > 2a$, for the simplified quadratic cloak.

One interesting observation from Figure 15 is that, for all three types of cloak, the scattering coefficient in each cylindrical order tends to converge to some specific value when $b \gg a$. For example, the zeroth-order scattering coefficient s_0 is approaching ~0.7, and s_1 is approaching ~0.16, etc. As the range of cloaks analyzed in this study is considered to be quite wide, the values suggest that the performances of simplified cloaks may have an upper limit. For the improved linear cloak and the simplified quadratic cloak, scattering is dominated by the zeroth-order component. For the originally proposed simplified linear cloak, relatively heavier scattering exists even when $b \gg a$. In addition, its scattered field is likely to comprise a significant portion of high-order cylindrical waves.

Knowing their inherent scattering properties, it is meaningful to verify the findings by some numerical experiments. Notice that scattering patterns obtained in such numerical experiments are source-dependent. Nevertheless they can qualitatively reflect the performances of the cloaks. Here a plane wave of unit amplitude is chosen as the incident wave in all calculations. The wave has $\lambda = 0.15$ m and travels from left to right. Three types of cloak are studied, including the previously proposed simplified linear cloak, improved linear cloak, and the simplified quadratic cloak, all with a PEC lining. For each type of cloak, two scales are examined. While a is kept constant at 0.1 m, b is at 0.15 m or 0.3 m. The calculated far field scattering patterns are summarized in Figure 16. For reference, the scattering pattern for a bare PEC cylinder with a 0.1 m radius is also imposed in the panels. All scattered far fields are normalized to the maximum scattered far field by the bare PEC cylinder.

For the previously proposed simplified linear cloak, the scattering remains high and varies wildly in angular direction, regardless of the cloak thickness. The sharp variation of the scattered field value in the angular direction suggests that the high-order cylindrical waves experience heavy scattering. By comparison, the improved linear cloak causes a relatively low scattering at all cloak thicknesses. The reduction in scattering is around 10dB in both the backward and forward directions as compared to the bare PEC cylinder. The relatively small angular dependence of the scattering pattern indicates that the scattering by such a cloak is dominated by the zeroth-order cylindrical wave. The quadratic cloak experiences heavy scattering when $b = 0.15$ m, which is almost as large as that caused by the bare PEC cylinder. This is due to violation of

Author's personal copy

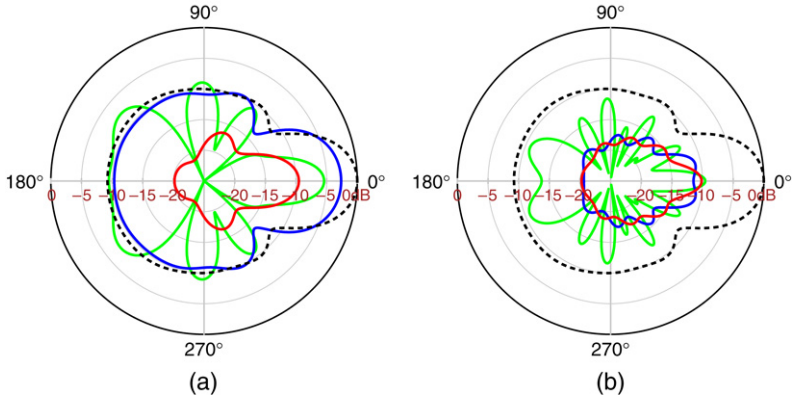

FIGURE 16 The far field scattering patterns by the simplified cloaks with an identical plane wave incidence (amplitude at 1). Green curves are for the previously proposed simplified linear cloak. Red curves are for the improved simplified linear cloak. Blue curves are for the simplified quadratic cloak. Dashed black curves are for the bare PEC cylinder. (a) $a = 0.1$ m, $b = 0.15$ m; (b) $a = 0.1$ m, $b = 0.3$ m. (For interpretation of the references to colour in this figure legend, the reader is referred to the web version of this article.)

the thickness constraint $b > 2a$. At $b = 0.3$ m, the scattering drops greatly, and becomes comparable to that caused by an improved linear cloak.

The E_z field patterns, together with the Poynting vectors for the three types of cloak, all with $a = 0.1$ m and $b = 0.3$m, are shown in Figure 17(a)–(c). In all cases a PEC lining is present. It is seen that all simplified cloaks cause perturbations to the plane wave. Nevertheless, all simplified cloaks are observed to imitate their respective ideal versions by bending the Poynting vectors around the inner shell and then returning the vectors back to their original trajectories. The perturbation caused by the previously proposed simplified linear cloak [Figure 17(a)] is larger than that caused by the improved linear cloak [Figure 17(b)]. By a careful comparison of fields in Figure 17(b) and (c), one can see that the quadratic cloak [Figure 17(c)] bends the EM field more severely at locations closer to the cloak's inner surface, whereas for the linear cloak [Figure 17(b)] the bending happens evenly at all radial locations. In all cases, the maximum field amplitude has increased from the ideal case, which is $-1 \rightarrow 1$. The scattered E_z fields by the three cloaks are plotted in Figure 17(d)–(f). The scattered field induced by the previously proposed simplified linear cloak [Figure 17(d)] is not only very high in amplitude, but also rather inhomogeneous angularly. By comparison, the scattered fields by the improved linear cloak [Figure 17(e)] and the simplified quadratic cloak [Figure 17(f)] are dominated by the zeroth-order cylindrical wave with

Author's personal copy

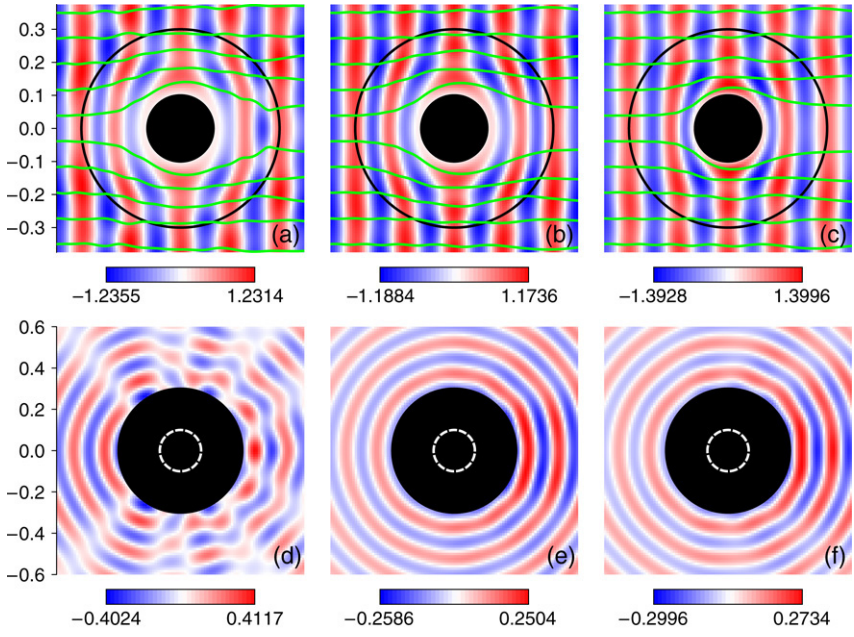

FIGURE 17 Snapshots of E_z fields around (a) a previously proposed simplified linear cloak, (b) an improved linear cloak, and (c) a simplified quadratic cloak. $a = 0.1\text{m}$, $b = 0.3\text{m}$. Poynting vectors are shown in green lines. The scattered E_z fields of the three cloaks in (a)–(c) are shown respectively in (d)–(f). Domain for (a)–(c): $0.75 \times 0.75\ \text{m}^2$, and for (d)–(f): $1.2 \times 1.2\ \text{m}^2$

significantly lower amplitude. These scattered near fields comply well with the results we obtained in Figures 15 and 16.

We conclude this subsection by stating that simplified cloaks with impedance-matched outer surfaces, in general, have better invisibility performance. However, it should be kept in mind that realization of such optimal models of simplified cloaks can be more difficult when compared to the one suggested in Schurig, Mock, Justice, Cummer, Pendry, Starr and Smith (2006a).

6. SPHERICAL INVISIBILITY CLOAK

Spherical cloaks have previously been studied in (Chen, Wu, Zhang and Kong, 2007b; Zhang, Chen, Wu and Kong, 2008a; Luo, Chen, Zhang, Ran and Kong, 2008).

A three-dimensional spherical cloak can be constructed by compressing the EM fields in a spherical region $r' < b$ into a spherical shell $a < r < b$. Here a generalized coordinate transformation where $r' = f(r)$ with

Author's personal copy

$f(a) = 0$ and $f(b) = b$ is considered. Therefore, a spherical cloak is indeed a special type of point-transformed cloak. The permittivity and permeability of the cloak, depending on r, are given as

$$\epsilon_r = \mu_r = \frac{f(r)^2}{r^2 f'(r)}, \quad \epsilon_\theta = \mu_\theta = \epsilon_\phi = \mu_\phi = f'(r). \tag{66}$$

Compared to ideal cylindrical cloaks, ideal spherical cloaks are more practical, since their material parameters don't have infinitely large values.

First, we look into the EM property of an ideal spherical cloak. Consider that fields $\mathbf{E}^i = [E_r^i, E_\theta^i, E_\phi^i]$ and $\mathbf{H}^i = [H_r^i, H_\theta^i, H_\phi^i]$ are incident upon the cloak. From Equation (13), the fields in the cloaked medium are obtained directly

$$\widehat{E}_r(r,\theta,\phi) = f'(r)E_r^i(f(r),\theta,\phi), \quad \widehat{H}_r(r,\theta,\phi) = f'(r)H_r^i(f(r),\theta,\phi), \tag{67}$$

$$\widehat{E}_\theta(r,\theta,\phi) = \frac{f(r)}{r}E_\theta^i(f(r),\theta,\phi), \quad \widehat{H}_\theta(r,\theta,\phi) = \frac{f(r)}{r}H_\theta^i(f(r),\theta,\phi), \tag{68}$$

$$\widehat{E}_\phi(r,\theta,\phi) = \frac{f(r)}{r}E_\phi^i(f(r),\theta,\phi), \quad \widehat{H}_\phi(r,\theta,\phi) = \frac{f(r)}{r}H_\phi^i(f(r),\theta,\phi). \tag{69}$$

At the inner boundary, observing Equations (68) and (69), the tangential components of the fields are zero. Combining this with $\epsilon_r = \mu_r = 0$, it can be seen that no field can penetrate the cloaked region.

For an ideal cylindrical cloak, it is known that a noticeable scattering will be induced if a thin layer is removed from the inner boundary. So we wonder whether the same phenomenon will occur for a spherical cloak. In the following, we will investigate such a problem. Considering Equation (66), we know that the wave in the cloak shell can be decoupled into spherical TE modes (the electric field has no $\hat{r}$ component) and spherical TM modes (the magnetic field has no $\hat{r}$ component). We consider the case where a TM wave is incident upon the cloak with a tiny perturbation. The results for a TE wave can be obtained in a similar way. The perturbation is again introduced by dislocating the cloak's inner interface from the ideal $r = a$ to $r = a + \delta$. The media inside the cloak shell is unknown, but with the assumption that the wave can be separated into TE and TM components. It is known that the wave in each region can be expressed by Debye potentials π_e, i.e., $B_{TM} = \nabla \times (r\pi_e)\widehat{r}$, $D_{TM} = \mathrm{i}\{\nabla \times [\overline{\overline{\mu}}^{-1} \cdot \nabla \times (r\pi_e)\widehat{r}]\}$. From Maxwell's equations, the Debye potentials in the outer free space

Author's personal copy

and the cloaked shell are obtained as

$$\pi_e = \sum_{n=1}^{+\infty}\sum_{m=-n}^{n} a^{in}_{(n,m)} j_n(k_0 r) P_n^m(\cos\theta)\mathrm{e}^{\mathrm{i}m\phi} + a^{sc}_{(n,m)} h_n(k_0 r) P_n^m(\cos\theta)\mathrm{e}^{\mathrm{i}m\phi} \quad (b < r), \tag{70}$$

$$\pi_e = \sum_{n=1}^{+\infty}\sum_{m=-n}^{n} \frac{f(r)f'(r)}{r}[a^1_{(n,m)} j_n(k_0 f(r)) + a^2_{(n,m)} h_n(k_0 f(r))] P_n^m(\cos\theta)\mathrm{e}^{\mathrm{i}m\phi} \quad (a+\delta < r < b). \tag{71}$$

In Equations (70) and (71), j_n and h_n represent the nth order spherical Bessel function of the first kind and nth order spherical Hankel function of the first kind, respectively; P_n^m represent the associated Legendre polynomials with order n and degree m; $a^{in}_{(n,m)}$ and $a^{sc}_{(n,m)}$ are the expansion coefficients for the Debye potentials of the incident and the scattered fields outside the cloak, respectively; and $a^i_{(n,m)}$ $(i = 1, 2)$ are the expansion coefficients for the the Debye potentials of the field in the cloak shell. H_θ and E_θ in the region $r < a + \delta$ are denoted by $H_\theta = \sum_{n=1}^{+\infty}\sum_{m=-n}^{n} a^3_{(n,m)} m S_n(r) P_n^m(\cos\theta)\mathrm{e}^{\mathrm{i}m\phi}/(\sin\theta\mu_0)$ and $E_\theta = \sum_{n=1}^{+\infty}\sum_{m=-n}^{n} a^3_{(n,m)} T_n(r) P_n^{m\,\prime}(\cos\theta)\mathrm{e}^{\mathrm{i}m\phi}/(-i\omega\epsilon_0)$, respectively, where $S_n(r)$ and $T_n(r)$ are determined by the media in the cloaked region. For isotropic homogenous media with relative permittivity ϵ_r and permeability μ_r, $S_n(r) = j_n(k_u r)/\mu_r$ and $T_n(r) = (j_n(k_u r)/r + k_u j_n'(k_u r))/(\epsilon_u\mu_u)$. If the cloaked media are inhomogeneous or anisotropic, close forms of $S_n(r)$ and $T_n(r)$ are difficult to obtain.

By considering the boundary conditions at $r = b$ and $r = a + \delta$, we obtain the scattering coefficient $C^{sc}_{n,m} = a^{sc}_{(n,m)}/a^{in}_{(n,m)}$ in an approximate form as

$$C^{sc}_{(n,m)} \approx \frac{\delta_f j_n(k_0\delta_f) T_n(a+\delta) - (k_0\delta_f j_n'(k_0\delta_f) + j_n(k_0\delta_f)) S_n(a+\delta)}{(k_0\delta_f h_n'(k_0\delta_f) + h_n(k_0\delta_f)) S_n(a+\delta) - \delta_f h_n(k_0\delta_f) T_n(a+\delta)}, \tag{72}$$

where δ_f is defined as the same as for the cylindrical cloak in Section 5.1. For the special case when a PEC (PMC) layer is put at $r = a + \delta$, Equation (72) is also valid by setting $S_n(a+\delta) = 1$ and $T(a) = 0$ for the PEC case ($S_n(a+\delta) = 0$ and $T(a) = 1$ for the PMC case). $C^{sc}_{n,m}$ is only dependent on n, so in the following discussions $C^{sc}_{n,m}$ is denoted by C^{sc}_n. Following the same procedure as for the cylindrical cloak, we find that the value of C^{sc}_n for the spherical cloak is mainly determined by $j_n(k_0\delta_f)/h_n(k_0\delta_f) \propto \delta^{(2n+1)p}$, which is independent of a, b, or the media in the cloaked region. To illustrate the convergence speed of C^{sc}_n for the spherical cloak, we plot $|C^{sc}_n|$ for $n = 1, 2$ versus δ in Figure 18(a) and (b)

Author's personal copy

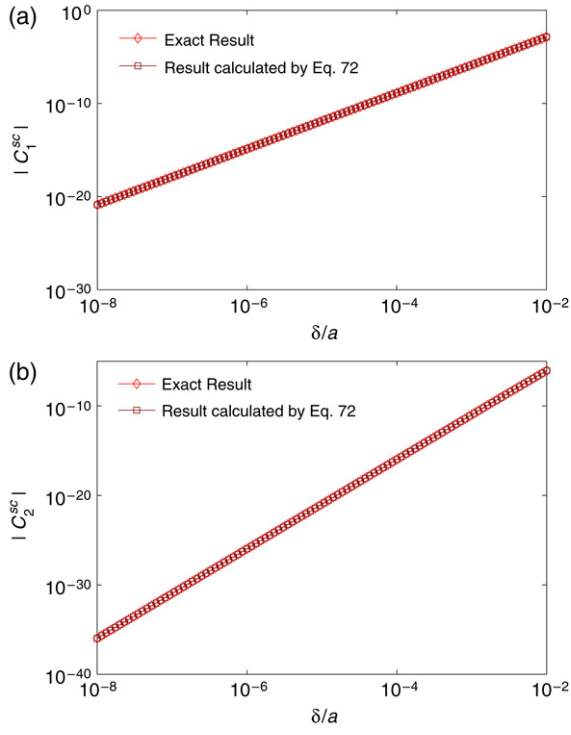

FIGURE 18 (a) $|C_1^{sc}|$ versus δ; (b) $|C_2^{sc}|$ versus δ. The spherical cloak is set $f(r) = b(r-a)/(b-a)$, $a = \pi/k_0$, $b = 2\pi/k_0$, and the region inside the cloak shell is air

with $f(r) = b(r-a)/(b-a)$, $a = \pi/k_0$, $b = 2\pi/k_0$, the region inside the cloak shell again being air. It is seen from Figure 18 that the exact result agrees well with the result calculated by Equation (72). The convergence speed of C_n^{sc} is found to be fast. Therefore the spherical cloak is not as sensitive to perturbation as the cylindrical cloak.

Despite the fact that the material parameters of a spherical cloak are all finite, the cloak's response to an active source located within the cloaked region is intriguing. This has been reported in Zhang, Chen, Wu and Kong (2008a), where the authors discussed the field solutions for a spherical invisibility cloak with an active device inside the cloaked region. It is found that no fields can escape from the cloaked region, i.e., invisibility cloaks can also cloak active objects. More interestingly, the tangential fields across the inner boundary of the cloak are discontinuous. It is obvious that this field discontinuity is not related to induced surface displacement currents (which result in the field discontinuity for the cylindrical cloak), since the components of permittivity and permeability

Author's personal copy

at the inner boundary of the spherical cloak are all finite, as seen from Equation (66). The true physical explanation is that the normal fields at the inner boundary of the cloak act as delta functions,which are caused by infinite polarizations of the material at the inner boundary of the spherical cloak. This explains the extraordinary electric and magnetic surface voltages at the inner boundary, as noticed by the authors in the aforementioned reference. From Faraday's law and Ampere's law, this extraordinary surface voltage will lead to the field discontinuity.

7. OTHER RELATED WORKS AND SOME PRACTICAL ISSUES

In this section, we mention some other related works on invisibility cloaks. Some practical issues concerning invisibility cloaks, including dispersion effects, material loss, and metamaterial technology development etc, will be addressed.

Apart from the previously mentioned cylindrical and spherical cloaks, invisibility cloaks with other shapes, such as elliptic or square, have also been theoretically demonstrated in published papers (Kwon and Werner, 2008; Ma, Qu, Xu, Zhang, Chen and Wang, 2008; Rahm, Schurig, Roberts, Cummer, Smith and Pendry, 2008b). Usually, cloaks are considered to operate in a homogenous and isotropic background. If the background is not homogenous and isotropic, such as cloaking on a dielectric half-space and cloaking in a photonic crystal, invisibility cloaks can also be designed based on the coordinate transformation method (Zhang, Huangfu, Luo, Chen, Kong and Wu, 2008b; Zhang, Jin and He, 2008c).

Our analyses presented in the above sections focus on the EM stable-state response of invisibility cloaks at a single operating frequency. The dispersion effects of cloaking materials are not considered. In practice, all material parameters in nature are dispersive. The effects induced by dispersion can't be neglected. Dynamical response and operating bandwidth are two issues closely related to dispersion (Liang, Yao, Sun and Jiang, 2008; Chen, Liang, Yao, Jiang, Ma, and Chan, 2007a). In Liang, Yao, Sun and Jiang (2008), the dynamical response of invisibility cloaks is investigated by the finite-difference time-domain (FDTD) method (simulation of invisibility cloaks using FDTD method is also presented in detail in Zhao, Argyropoulos and Hao (2008)). It is found that there is a strong scattering process before a dispersive cloak achieves its stable state (cloaking state). This strong scattering phenomenon is due to the existence of material dispersion. The time length of this dynamical process, called "relaxation time", depends on the dispersion. A weaker dispersion leads to a shorter relaxation time. In a dynamical process, the EM field is usually not of a single frequency, but consists of a broad frequency spectrum. The ideal material parameters for achieving perfect invisibility can't be

Author's personal copy

satisfied at all frequency values, due to inevitable material dispersion and as a consequence, scattering is likely to occur. The presence of material dispersion is the key factor that technologically prevents broadband invisibility operation.

To realize a practical invisibility cloak, the metamaterial technology can be applied to engineer material parameters. Metamaterials are usually constructed by periodic metal resonators with a periodicity much smaller than the wavelength. Each resonator operates effectively as an electric dipole or a magnetic dipole to induce electric or magnetic responses. So far, a variety of metamaterial structures have been proposed in the microwave regime (Falcone, Lopetegi, Laso, Baena, Bonache, Beruete, Marqués, Martín and Sorolla, 2004; Pendry, Holden, Stewart and Youngs, 1996; Pendry, Holden, Robbins and Stewart, 1999). More recently, metamaterials operating at optical frequency have also been reported. Metamaterials with magnetic response at optical frequency have been reported in Dolling, Enkrich, Wegener, Zhou, Soukoulis and Linden (2005), Dolling, Enkrich, Wegener, Soukoulis and Linden (2006), Shalaev, Cai, Chettiar, Yuan, Sarychev, Drachev and Kildishev (2005) and Shalaev (2006). Thus, invisibility cloaks operating at optical frequency are possible. However, it should be pointed out that the resonance-based metamaterials are inherently lossy, especially at the optical frequency. The presence of imaginary parts in the permittivity and permeability values is another key restriction that limits the invisibility performance of cloaking devices. Engineering metamaterial with low loss is still a challenging task and is currently under extensive research.

8. CONCLUSION

A detailed summary of invisibility cloaking technology, including theory, material simplification, and practical realization has been given in this article. Transformation optics provides a rather effective approach for designing such an invisibility cloak, and even for a broader class of functioning electromagnetic media, called transformation media. With the advances in metamaterial fabrication technology, it is now possible to realize the designed invisibility cloaks.

The electromagnetic properties of a general ideal invisibility cloak have been investigated. By dividing cloaks into two types: line-transformed cloaks and point-transformed cloaks, we notice that:

(1) No reflection is excited at both outer and inner boundaries of ideal invisibility cloaks, and no field can penetrate into the cloaked region. That is, ideal invisibility cloaks by coordinate transformation are perfectly invisible.

Author's personal copy

(2) For a line-transformed ideal cloak, material parameters at the inner boundary always have infinitely large components. There exists a field discontinuity across the inner boundary. The surface displacement currents are induced to make this discontinuity self-consistent.
(3) For a point-transformed ideal cloak, material parameters at the inner boundary do not have infinitely large components, the components in the normal direction of the inner boundary are always zero, and the fields are continuous across the inner boundary.

Special attention has been paid to cylindrical invisibility cloaks, since they are arguably the simplest structure in terms of realization. The main properties of cylindrical cloaks are listed as follows:

(1) An ideal cylindrical cloak is very sensitive to geometrical perturbations at the inner boundary.
(2) This sensitive problem can be overcome by imposing a PEC (PMC) layer at the inner boundary of the cloak for TM (TE) polarization operation.
(3) A simplified cloak is inherently visible.
(4) If the outer boundary of a simplified cloak is matched with free space, scattering of high order cylindrical waves can be reduced dramatically.

Spherical cloaks have also been discussed. It was concluded that ideal spherical cloaks are not sensitive to perturbations at the inner boundary.

Some practical issues concerning invisibility cloaks, including dispersion, loss, and practical realization, have been addressed. The performance of invisibility cloaks is limited by both material dispersion and loss. Realization of high-performance invisibility cloaks relies critically on metamaterial design and fabrication technologies.

ACKNOWLEDGEMENT

This work has been supported by the Swedish Foundation for Strategic Research (SSF) through the Future Research Leader program, the SSF Strategic Research Center in Photonics, and the Swedish Research Council (VR).

REFERENCES

Alù, A. and Engheta, N. (2005). Achieving transparency with plasmonic and metamaterial coatings. *Physical Review E*, 72, 016623. July.

Alù, A. and Engheta, N. (2008). Multifrequency optical invisibility cloak with layered plasmonic shells. *Physical Review Letters*, 100 (11), 113901.

Arfken, G. (1970). *Mathematical Methods for Physicists*, second edition. Academic Press (chapter 9).

Author's personal copy

Cai, W., Chettiar, U. K., Kildishev, A. V. and Shalaev, V. M. (2007a). Optical cloaking with metamaterials. *Nature Photonics*, 1, 224–227, April.

Cai, W., Chettiar, U. K., Kildishev, A. V., Shalaev, V. M. and Milton, G. W. (2007b). Nonmagnetic cloak with minimized scattering. *Applied Physics Letters*, 91 (11), 111105.

Chen, H. and Chan, C. T. (2007). Transformation media that rotate electromagnetic fields. *Applied Physics Letters*, 90 (24), 241105.

Chen, H., Liang, Z., Yao, P., Jiang, X., Ma, H. and Chan, C. T. (2007a). Extending the bandwidth of electromagnetic cloaks. *Physical Review B*, 76 (24), 241104(R).

Chen, H., Wu, B.-I., Zhang, B. and Kong, J. A. (2007b). Electromagnetic wave interactions with a metamaterial cloak. *Physical Review Letters*, 99 (6), 063903.

Chen, H.-Y., Yang, T., Luo, X.-D. and Ma, H.-R. (2008). The impedance-matched reduced acoustic cloaking with realizable mass and its layered design. arXiv:0805.1114v1 [cond-mat.mtrl-sci].

Cummer, S. A., Popa, B.-I., Schurig, D., Smith, D. R. and Pendry, J. (2006). Full-wave simulations of electromagnetic cloaking structures. *Physical Review E*, 74 (3), 036621.

Cummer, S. A., Popa, B.-I., Schurig, D., Smith, D. R., Pendry, J., Rahm, M. and Starr, A. (2008). Scattering theory derivation of a 3d acoustic cloaking shell. *Physical Review Letters*, 100 (2), 024301.

Cummer, S. A. and Schurig, D. (2007). One path to acoustic cloaking. *New Journal of Physics*, 9 (3), 45.

Dolling, G., Enkrich, C., Wegener, M., Soukoulis, C. M. and Linden, S. (2006). Simultaneous negative phase and group velocity of light in a metamaterial. *Science*, 312 (5775), 892–894.

Dolling, G., Enkrich, C., Wegener, M., Zhou, J. F., Soukoulis, C. M. and Linden, S. (2005). Cut-wire pairs and plate pairs as magnetic atoms for optical metamaterials. *Optics Letters*, 30 (23), 3198–3200.

Falcone, F., Lopetegi, T., Laso, M. A. G., Baena, J. D., Bonache, J., Beruete, M., Marqués, R., Martín, F. and Sorolla, M. (2004). Babinet principle applied to the design of metasurfaces and metamaterials. *Physical Review Letters*, 93 (19), 197401. Nov.

Farhat, M., Enoch, S., Guenneau, S. and Movchan, A. B. (2008). Broadband cylindrical acoustic cloak for linear surface waves in a fluid. *Physical Review Letters*, 101 (13), 134501.

Felbacq, D., Tayeb, G. and Maystre, D. (1994). Scattering by a random set of parallel cylinder. *Journal of the Optical Society of America A*, 11 (9), 2526–2538, September.

Greenleaf, A., Kurylev, Y., Lassas, M. and Uhlmann, G. (2007a). Electromagnetic wormholes and virtual magnetic monopoles from metamaterials. *Physical Review Letters*, 99 (18), 183901.

Greenleaf, A., Kurylev, Y., Lassas, M. and Uhlmann, G. (2007b). Full-wave invisibility of active devices at all frequencies. *Communications in Mathematical Physics*, 275, 749–789.

Greenleaf, A., Kurylev, Y., Lassas, M. and Uhlmann, G. (2007c). Improvement of cylindrical cloaking with the shs lining. *Optics Express*, 15 (20), 12717–12734.

Greenleaf, A., Kurylev, Y., Lassas, M. and Uhlmann, G. (2008). Approximate quantum cloaking and almost trapped states. arXiv:0806.0368v1[quant-ph].

Greenleaf, A., Lassas, M. and Uhlmann, G. (2003). Anisotropic conductivities that cannot be detected by eit. *Physiological Measurement*, 24, 413–419.

Kildishev, A. V. and Narimanov, E. E. (2007). Impedance-matched hyperlens. *Optics Letters*, 32 (23), 3432–3434, December.

Kildishev, A. V. and Shalaev, V. M. (2008). Engineering space for light via transformation optics. *Optics Letters*, 33 (1), 43–45, December.

Kong, F., Wu, B.-I., Kong, J. A., Huangfu, J., Xi, S. and Chen, H. (2007). Planar focusing antenna design by using coordinate transformation technology. *Applied Physics Letters*, 91 (25), 253509.

Kwon, D.-H. and Werner, D. H. (2008). Two-dimensional eccentric elliptic electromagnetic cloaks. *Applied Physics Letters*, 92 (1), 013505.

Leonhardt, U. (2006). Optical conformal mapping. *Science*, 312, 1777–1780, June.

Author's personal copy

Leonhardt, U. and Philbin, T. G. (2006). General relativity in electrical engineering. *New Journal of Physics*, 8, 247. October.

Leonhardt, U. and Philbin, T. G. (2008). Transformation optics and the geomety of light. arXiv:0805.4778v2.

Liang, Z., Yao, P., Sun, X. and Jiang, X. (2008). The physical picture and the essential elements of the dynamical process for dispersive cloaking structures. *Applied Physics Letters*, 92 (13), 131118.

Luo, Y., Chen, H., Zhang, J., Ran, L. and Kong, J. A. (2008). Design and analytical full-wave validation of the invisibility cloaks, concentrators, and field rotators created with a general class of transformations. *Physical Review B (Condensed Matter and Materials Physics)*, 77 (12), 125127.

Ma, H., Qu, S., Xu, Z., Zhang, J., Chen, B. and Wang, J. (2008). Material parameter equation for elliptical cylindrical cloaks. *Physical Review A (Atomic, Molecular, and Optical Physics)*, 77 (1), 013825.

Miller, D. A. B. (2006). On perfect cloaking. *Optics Express*, 15, 12457–12466, December.

Milton, G. W., Briane, M. and Willis, J. R. (2006). On cloaking for elasticity and physical equations with a transformation invariant form. *New Journal of Physics*, 8 (10), 248.

Milton, G. W. and Nicorovici, N.-A. P. (2006). On the cloaking effects associated with anomalous localized resonance. *Proceedings of the Royar Society of London, Series A*, 462, 3027–3059.

Nicolet, A., Zolla, F. and Guenneau, S. (2004). Modelling of twisted optical waveguides with edge elements. *The European Physical Journal of Applied Physics*, 28, 153157.

Norris, A.N. (2008). Acoustic cloaking in 2d and 3d using finite mass. arXiv:0802.0701v1 [physics.flu-dyn].

Pendry, J., Holden, A., Robbins, D. and Stewart, W. (1999). Magnetism from conductors and enhanced nonlinear phenomena. *Microwave Theory and Techniques, IEEE Transactions on*, 47 (11), 2075–2084, Nov. (ISSN: 0018-9480).

Pendry, J. B. (2000). Negative refraction makes a perfect lens. *Physical Review Letters*, 85 (18), 3966–3969, October.

Pendry, J. B., Holden, A. J., Stewart, W. J. and Youngs, I. (1996). Extremely low frequency plasmons in metallic mesostructures. *Physical Review Letters*, 76 (25), 4773–4776, Jun.

Pendry, J. B., Schurig, D. and Smith, D. R. (2006). Controlling electromagnetic fields. *Science*, 312 (5781), 1780–1782, June.

Post, E. J. (1962). *Formal Structure of Electromagnetics*. North-Holland publishing company, Amsterdam.

Rahm, M., Cummer, S. A., Schurig, D., Pendry, J. B. and Smith, D. R. (2008a). Optical design of reflectionless complex media by finite embedded coordinate transformations. *Physical Review Letters*, 100 (6), 063903.

Rahm, M., Schurig, D., Roberts, D. A., Cummer, S. A., Smith, D. and Pendry, J. B. (2008b). Design of electromagnetic cloaks and concentrators using form-invariant coordinate transformations of Maxwell's equations. *Photonics and Nanostructures - Fundamentals and Applications*, 6, 87–95.

Ruan, Z., Yan, M., Neff, C. W. and Qiu, M. (2007). Ideal cylindrical cloak: Perfect but sensitive to tiny perturbations. *Physical Review Letters*, 99 (11), 113903.

Schurig, D., Mock, J. J., Justice, B. J., Cummer, S. A., Pendry, J. B., Starr, A. F. and Smith, D. R. (2006a). Metamaterial electromagnetic cloak at microwave frequencies. *Science*, 314 (5801), 977–980, November.

Schurig, D., Pendry, J. B. and Smith, D. R. (2006b). Calculation of material properties and ray tracing in transformation media. *Optics Express*, 14 (21), 9794–9804.

Schurig, D., Pendry, J. B. and Smith, D. R. (2007). Transformation-designed optical elements. *Optics Express*, 15 (22), 14772–14782.

Shalaev, V. M. (2006). Optical negative-index metamaterials. *Nature Photonics*, 1, 41–48.

Author's personal copy

Shalaev, V. M., Cai, W., Chettiar, U. K., Yuan, H.-K., Sarychev, A. K., Drachev, V. P. and Kildishev, A. V. (2005). Negative index of refraction in optical metamaterials. *Optics Letters*, 30 (24), 3356–3358.

Shelby, R. A., Smith, D. R. and Schultz, S. (2001). Experimental Verification of a Negative Index of Refraction. *Science*, 292 (5514), 77–79.

Shyroki, D. M. (2008). Exact equivalent straight waveguide model for bent and twisted waveguides. *IEEE Transactions on Microwave Theory and Techniques*, 56 (2), 414–419, February.

Smith, D. R., Pendry, J. B. and Wiltshire, M. C. K. (2004). Metamaterials and Negative Refractive Index. *Science*, 305 (5685), 788–792.

Tsang, M. and Psaltis, D. (2008). Magnifying perfect lens and superlens design by coordinate transformation. *Physical Review B (Condensed Matter and Materials Physics)*, 77 (3), 035122.

Ward, A. J. and Pendry, J. B. (1996). Refraction and geometry in maxwell's equations. *Journal of Modern Optics*, 43 (4), 773–793.

Yan, M., Ruan, Z. and Qiu, M. (2007a). Cylindrical invisibility cloak with simplified material parameters is inherently visible. *Physical Review Letters*, 99 (23), 233901.

Yan, M., Ruan, Z. and Qiu, M. (2007b). Scattering characteristics of simplified cylindrical invisibility cloaks. *Optics Express*, 15 (26), 17772–17782.

Yan, M., Yan, W. and Qiu, M. (2008a). Cylindrical superlens by a coordinate transformation. *Physical Review B*, 78 (12), 125113.

Yan, W., Yan, M. and Qiu, M. (2008b). Necessary and sufficient conditions for reflectionless transformation media in an isotropic and homogenous background. arXiv:0806.3231v1.

Yan, W., Yan, M., Ruan, Z. and Qiu, M. (2008c). Coordinate transformations make perfect invisibility cloaks with arbitrary shape. *New Journal of Physics*, 10 (4), 043040. 13pp.

Yan, W., Yan, M., Ruan, Z. and Qiu, M. (2008d). Influence of geometrical perturbation at inner boundaries of invisibility cloaks. *Journal of the Optical Society of America, Series A*, 25 (4), 968–973.

Zhang, B., Chen, H., Wu, B.-I., Luo, Y., Ran, L. and Kong, J. A. (2007). Response of a cylindrical invisibility cloak to electromagnetic waves. *Physical Review B (Condensed Matter and Materials Physics)*, 76 (12), 121101.

Zhang, B., Chen, H., Wu, B.-I. and Kong, J. A. (2008a). Extraordinary surface voltage effect in the invisibility cloak with an active device inside. *Physical Review Letters*, 100 (6), 063904.

Zhang, J., Huangfu, J., Luo, Y., Chen, H., Kong, J. A. and Wu, B.-I. (2008b). Cloak for multilayered and gradually changing media. *Physical Review B*, 77, 035116.

Zhang, P., Jin, Y. and He, S. (2008c). Cloaking an object on a dielectric half-space. *Optics Express*, 16 (5), 3161–3166.

Zhang, S., Genov, D. A., Sun, C. and Zhang, X. (2008d). Cloaking of matter waves. *Physical Review Letters*, 100 (12), 123002.

Zhao, Y., Argyropoulos, C. and Hao, Y. (2008). Full-wave finite-difference time-domain simulation of electromagnetic cloaking structures. *Optics Express*, 16 (9), 6717–6730.

Zolla, F., Guenneau, S., Nicolet, A. and Pendry, J. B. (2007). Electromagnetic analysis of cylindrical invisibility cloaks and the mirage effect. *Optics Letters*, 32 (9), 1069–1071.